ARTICLES
https://doi.org/10.1038/s41556-017-0011-1
nature cell biology

Unresolved recombination intermediates lead to ultra-fine anaphase bridges, chromosome breaks and aberrations

Ying Wai Chan, Kasper Fugger and Stephen C. West*

The resolution of joint molecules that link recombining sister chromatids is essential for chromosome segregation. Here, we determine the fate of unresolved recombination intermediates arising in cells lacking two nucleases required for resolution (*GEN1*$^{-/-}$ knockout cells depleted of MUS81). We find that intermediates persist until mitosis and form a distinct class of anaphase bridges, which we term homologous recombination ultra-fine bridges (HR-UFBs). HR-UFBs are distinct from replication stress-associated UFBs, which arise at common fragile sites, and from centromeric UFBs. HR-UFBs are processed by BLM helicase to generate single-stranded RPA-coated bridges that are broken during mitosis. In the next cell cycle, DNA breaks activate the DNA damage checkpoint response, and chromosome fusions arise by non-homologous end joining. Consequently, the cells undergo cell cycle delay and massive cell death. These results lead us to present a model detailing how unresolved recombination intermediates can promote DNA damage and chromosomal instability.

Proper chromosome segregation depends on the removal of all physical connections between sister chromatids before anaphase. These connections can be proteinaceous, such as cohesin linkages[1], or might be mediated through DNA bridges that are a potential source of genome instability[2]. Sister chromatid non-disjunction can manifest as fine DNA strands between segregating DNA masses. These DNA strands are referred to as ultra-fine DNA bridges (UFBs) and cannot be visualized using standard DNA dyes (for example, DAPI), but can be detected by immunofluorescence staining for proteins such as PICH (PLK1-interacting checkpoint helicase), BLM (Bloom's syndrome helicase) and RPA (replication protein A), which bind the bridge[3–6]. Three major types of UFB have been described[7]: centromeric UFBs (C-UFBs), replication stress UFBs (FS-UFBs) and telomeric UFBs (T-UFBs). C-UFBs, which are the most common UFBs, originate in centromeric regions and involve double-stranded catenanes that are resolved by topoisomerase II[8,9]. FS-UFBs can arise from late replication intermediates at common fragile sites (CFSs) following replication stress, and are characterized by the presence of twin FANCD2 repair foci[7,10–13]. T-UFBs develop due to replication stalling or fusion events occurring at telomeric sequences[14–16].

Intermediates of homologous recombination provide a covalent link between sister chromatids and cause chromosome segregation defects if not removed before anaphase[17]. In human cells, multiple mechanisms have evolved to process recombination intermediates. One mechanism involves the BTR complex (BLM–TOPOIIIα–RMI1–RMI2), which mediates the dissolution of double Holliday junctions[18]. Persistent double Holliday junctions and other types of recombination intermediates (for example, single HJs and D-loop structures) that are refractory to dissolution are resolved by structure-selective endonucleases (SSEs). These SSEs include MUS81–EME1[19,20], SLX1–SLX4[21–23] and GEN1[24–26]. SLX1–SLX4 forms a complex with MUS81–EME1 and a third nuclease, XPF-ERCC1, to form the SMX tri-nuclease complex[27,28]. The SMX complex and GEN1 cleave recombination intermediates via two genetically distinct resolution pathways[17,28–31].

Distinct regulatory mechanisms restrain the actions of SSEs to the later stages of the cell cycle. The formation of the SMX complex occurs at prometaphase following CDK1- and PLK1-directed phosphorylation of MUS81–EME1 and SLX4[28,32]. The formation of the SMX complex activates MUS81–EME1 for cleaving persistent recombination and replication intermediates[27]. GEN1 acts later in the cell cycle, as this primarily cytoplasmic protein gains access to the remaining DNA intermediates after the nuclear envelope breaks down upon mitotic entry[33,34]. Cells defective for resolution exhibit chromosome segregation errors and reduced viability[17,28–31].

Here, we establish a 'resolvase-deficient' model system to examine what happens when cells with unresolved recombination intermediates enter mitosis. We find that recombination intermediates produce UFBs that we term homologous recombination-UFBs (HR-UFBs). BLM helicase activity is required for the conversion of the recombination intermediates into RPA-coated single-stranded bridges that are broken upon cell division. This event leads to chromosome aberrations and activation of the DNA damage checkpoint response in the next cell cycle.

Results

Resolvase-deficiency promotes cell cycle arrest and cell death. To determine the consequences of aberrant mitosis caused by unresolved recombination intermediates, we established a resolvase-deficient experimental system in cultured human cells. Short interfering RNA (siRNA) was used to deplete MUS81 from a *GEN1*$^{-/-}$ knockout cell line generated from 293 cells using CRISPR (clustered regularly interspaced short palindromic repeats)–Cas9 technology[34] (Fig. 1a). The resolvase-deficient cells exhibited a reduced frequency of sister chromatid exchanges (SCEs) compared with *GEN1*$^{-/-}$ cells or MUS81-depleted normal cells (Supplementary Fig. 1a). These data confirm that resolvases are responsible for generating crossovers[17,28–31].

The resolvase-deficient cells exhibited a series of striking phenotypic properties. First, we observed an accumulation of cells with 4N DNA content (Fig. 1b,c). To confirm G2 arrest, cells were

The Francis Crick Institute, London, UK. *e-mail: stephen.west@crick.ac.uk

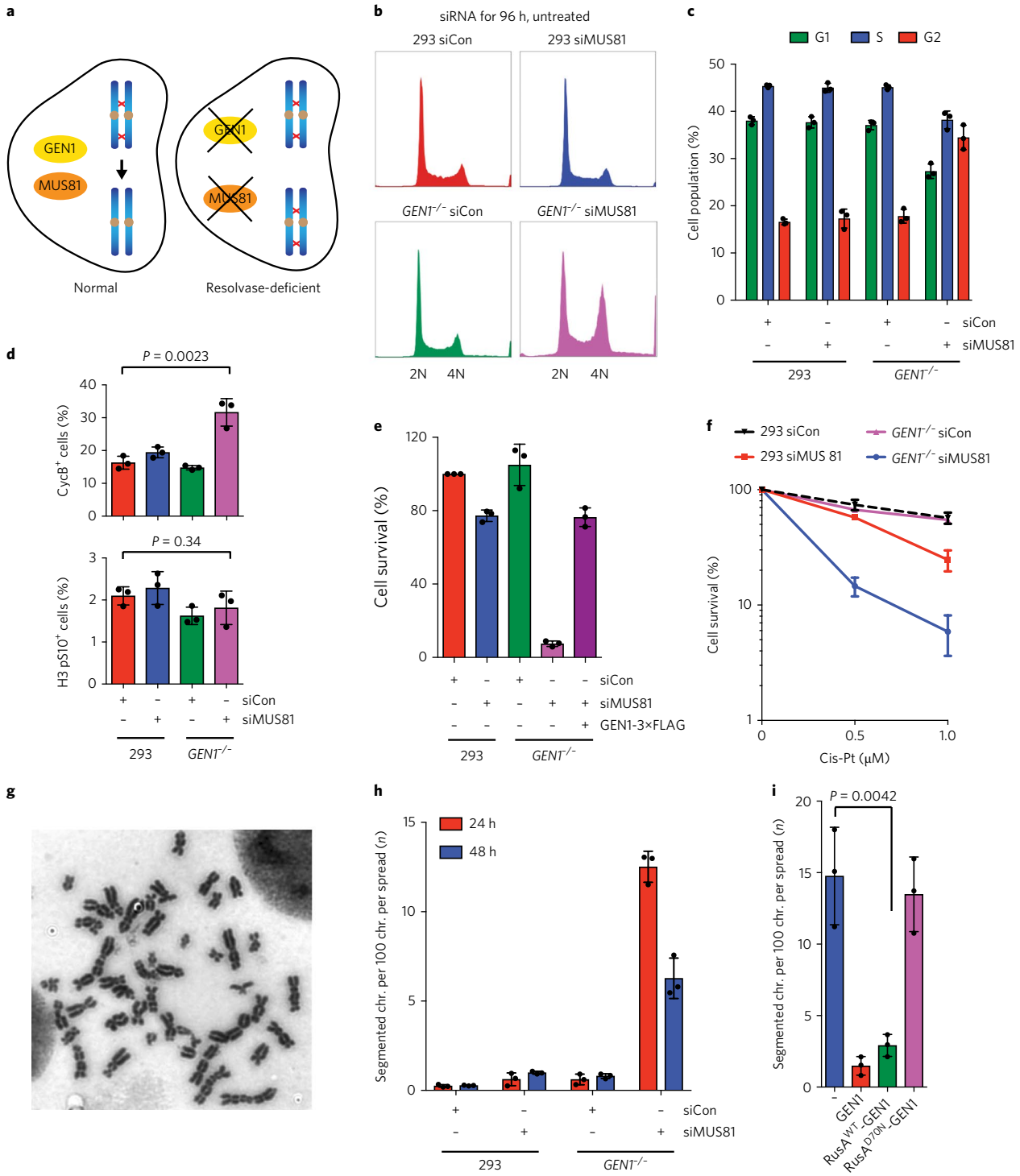

Fig. 1 | Phenotypic analysis of resolvase-deficient cells. a, Schematic depicting the experimental system. **b**, *GEN1*$^{-/-}$ cells and 293 cells were treated with control siRNA (siCon) or siRNA against *MUS81* (siMUS81) for 96 h. FACS results show their DNA content distributions. **c**, Quantification of G1, S and G2 populations of cells treated as in **b**. **d**, Cells were treated as in **b** and stained with a cyclin B-specific antibody (upper panel) or a histone H3 pSer10-specific antibody (lower panel). Percentages of cyclin B-positive (CycB^{+}) and histone H3 pSer10-positive (H3 pS10^{+}) cells were quantified. **e**, Clonogenic cell survival assays were carried out on 293 cells and *GEN1*$^{-/-}$ cells treated with control siRNA or siRNA against *MUS81*. Complementation via the stable expression of GEN1-3× FLAG is indicated. The survival of control siRNA-treated 293 cells is defined as 100%. **f**, Clonogenic cell survival assays were carried out on 293 cells and *GEN1*$^{-/-}$ cells treated with control siRNA or siRNA against *MUS81* and the indicated concentrations of cisplatin (Cis-Pt). **g**, Chromosome segmentation in a metaphase spread from *GEN1*$^{-/-}$ cells treated with siRNA against *MUS81* and a brief (1 h) cisplatin treatment and then released into fresh media for 24 h. **h**, *GEN1*$^{-/-}$ cells and 293 cells were treated as in **g** but released into fresh media for 24 h (red) or 48 h (blue). A total of 75 metaphase spreads per condition were analysed for chromosome (chr.) segmentation. **i**, *GEN1*$^{-/-}$ (−) and *GEN1*$^{-/-}$ cells expressing GEN1, RusA^{WT}-GEN1 or RusA^{D70N}-GEN1 as indicated were treated as in **g**. A total of 60 metaphase spreads per condition were analysed for chromosome segmentation. In **b** and **g**, representative data from three independent experiments are shown. Quantified data in **c**–**f**, **h** and **i** represent the mean ± s.d. of $n = 3$ independent experiments. Source data are available in Supplementary Table 1. *P* values were determined using a two-tailed *t*-test.

treated with antibodies against cyclin B (a G2 marker) and histone H3 pSer10 (a mitotic marker), and analysed by fluorescence-activated cell sorting (FACS) (Fig. 1d). A significant increase in cyclin B-positive cells, but not histone H3 pSer10-positive cells, was observed. G2 arrest occurred 96 h after *MUS81* siRNA treatment of the *GEN1*$^{-/-}$ cells (Supplementary Fig. 1b), indicating the accumulation of endogenous DNA damage. Furthermore, clonogenic assays showed massive synthetic lethality (<10% cell survival) (Fig. 1e). Loss of viability and G2 arrest were rescued through the exogenous expression of FLAG-tagged GEN1 (Fig. 1e and Supplementary Fig. 1c,d). The resolvase-deficient cells were highly sensitive to the DNA-damaging agents cisplatin and camptothecin (Fig. 1f and Supplementary Fig. 1e), but only mildly sensitive to aphidicolin-induced replication stress (Supplementary Fig. 1f). These results are consistent with those demonstrating the involvement of MUS81–EME1 and GEN1 in the resolution of DNA repair intermediates.

To gain further insights into the interplay between GEN1 and components of the SMX complex (in particular MUS81–EME1 and SLX1–SLX4), *MUS81*$^{-/-}$ and *SLX1*$^{-/-}$ knockout cells were generated using CRISPR/Cas9 technology (Supplementary Fig. 1g–i). Depletion of GEN1 from *MUS81*$^{-/-}$ cells induced massive cell death and severe G2 arrest (Supplementary Fig. 2a,b), whereas a less significant effect was seen in GEN1-depleted *SLX1*$^{-/-}$ cells. This result indicates that SLX1 may only be required for the resolution of a subset of repair intermediates. Consistent with this notion, G2 arrest and lethality was further exacerbated when both SLX1 and MUS81 were depleted in *GEN1*$^{-/-}$ cells (Supplementary Fig. 2c,d).

The interaction between MUS81 and the SLX4 scaffold protein is crucial for resolution events mediated by SMX [27,30,31,35]. We therefore mutated the key conserved residues in SLX4 (E1577A and L1578A) that are equivalent to those previously identified in mouse SLX4 and shown to abolish MUS81–SLX4 interactions[30] (Supplementary Fig. 2e). We observed that depletion of GEN1 in SLX4$^{E1577A\ L1578A}$ (SLX4^{ELAA}) cells induced cell death and cell cycle arrest (Supplementary Fig. 2f–h). These results confirm the synthetic relationship between GEN1 and SMX complex.

Unresolved recombination intermediates form UFBs. To investigate the consequences of mitosis in cells with unresolved recombination intermediates, we briefly treated resolvase-deficient cells with cisplatin and prepared metaphase spreads 24 h later. We observed tightly associated sister chromatids that exhibited a segmented appearance (Fig. 1g,h). This unusual morphology was previously attributed to defects in chromosome condensation at sites of sister chromatid entanglements[17,29,31]. Increased levels of chromosome segmentation were observed in the resolvase-deficient cells even in the absence of exogenous damage (Supplementary Fig. 3a). Segmentation was suppressed in cells expressing the bacterial resolvase RusA fused to catalytic-dead GEN1 (with E134A and E136A mutations) to ensure correct cellular regulation, but not in cells expressing catalytic-dead RusA^{D70N}–GEN1 (Fig. 1i and Supplementary Fig. 3b,c). Indeed, RusA^{WT}–GEN1 rescued all other phenotypes associated with resolvase deficiency, namely reduced SCE formation (Supplementary Fig. 3d) and G2 arrest (Supplementary Fig. 3e). These results show that the uncondensed regions arise from unresolved intermediates that interlink sister chromatids.

As unresolved recombination intermediates do not trigger the cell cycle checkpoint response, the sister chromatid linkages persist to anaphase. Consequently, ~80% of the resolvase-deficient cells (undamaged or cisplatin-treated) displayed RPA-decorated UFBs at anaphase/telophase compared with ~10–15% in control and single resolvase-depleted cells (Fig. 2a,b and Supplementary Fig. 3f–h). The binding of RPA indicates that the bridges contain single-stranded DNA (ssDNA). Mild replication stress (for example, exposure to low-dose aphidicolin) has been shown to lead to unresolved replication intermediates at CFSs. These unresolved replication intermediates give rise to FS-UFBs exhibiting RPA and BLM staining, and with twin FANCD2 foci at their termini[5,10,11]. In contrast to FS-UFBs, we observed UFBs that were not flanked by FANCD2; ~5% of mock-depleted wild-type cells and ~70% of the resolvase-deficient cells displayed FANCD2-negative UFBs (Fig. 2a,b and Supplementary Fig. 3f–h). These UFBs therefore appear to represent a distinct class of UFB, which we term HR-UFBs.

To determine whether the UFBs that arise in resolvase-deficient 293 cells were representative of those in all cell types, GEN1 and MUS81 were depleted from the non-transformed diploid cell line hTERT-RPE1. Again, we observed an increase in FANCD2-negative UFBs compared with control and single-resolvase depleted cells (Fig. 2g,h and Supplementary Fig. 3i). These HR-UFBs did not associate with centromeres, as detected by CREST staining (Supplementary Fig. 3j).

In addition to RPA, the UFBs were also decorated with BLM (Supplementary Fig. 4a,b). To confirm that the RPA- and BLM-coated UFBs did not associate with FANCD2 foci or centromeres, we co-stained for RPA and BLM and either FANCD2 or CREST using U2OS cells depleted of MUS81 and GEN1 (Supplementary Fig. 4a,b). We again observed that the majority of the RPA- and BLM-coated UFBs did not associate with FANCD2 (41 out of 49 UFBs were FANCD2 negative; 20 cells counted) or centromeres (34 out of 47 UFBs failed to show any association with CREST; 20 cells counted).

To provide further support for the distinction between HR-UFBs and FS-UFBs, we investigated whether FANCD2 twin foci and DNA synthesis (as indicated by EdU incorporation)[12,13,36], occur at prometaphase in the resolvase-deficient cells. As expected, control cells treated with aphidicolin exhibited an increased frequency of FANCD2 twin foci and EdU foci on their mitotic chromosomes (Fig. 2c,d and Supplementary Fig. 4c,d), whereas brief cisplatin treatment of the resolvase-deficient cells did not lead to detectable replication stress (as indicated by FANCD2 analysis and EdU staining). Moreover, DNA fibre analysis indicated that untreated resolvase-deficient cells did not show reduced replication progression (Fig. 2e,f), confirming that the HR-UFBs are not induced by replication stress.

To extend our analysis of HR-UFBs, we compared resolvase-deficient cells treated with aphidicolin, or camptothecin which causes replication fork collapse and double-strand break formation (Fig. 3a,b and Supplementary Fig. 4e,f). Aphidicolin treatment increased the number of FANCD2-positive UFBs whereas the number of FANCD2-negative HR-UFBs remained unchanged. In contrast, camptothecin treatment induced both types of UFBs, indicating that collapsed forks and double-strand breaks lead to the formation of recombination intermediates that require processing.

To confirm that the UFBs described here are generated by homologous recombination, we depleted RAD51 or BRCA2 (Supplementary Fig. 4g). As inactivation of RAD51 or BRCA2 can also induce replication stress[10,37], FANCD2-positive and FANCD2-negative UFBs were quantified. Depletion of RAD51 or BRCA2 reduced the number of FANCD2-negative UFBs (that is, HR-UFBs) and increased the number of FANCD2-positive UFBs (Fig. 3c,d). Expression of RusA^{WT}–GEN1, but not RusA^{D70N}–GEN1, reduced UFB formation in the resolvase-deficient cells (Fig. 3e,f and Supplementary Fig. 4h,i), further supporting the concept that these UFBs are generated by homologous recombination.

HR-UFB breakage promotes DNA damage and chromosome abnormalities. As UFBs were not observed in resolvase-deficient cells that had completed cytokinesis (Supplementary Fig. 5a), we reasoned that the single-stranded HR-UFBs are likely to be fragile and could be broken by the spindle forces present at mitosis. We therefore determined the levels of DNA damage in the subsequent

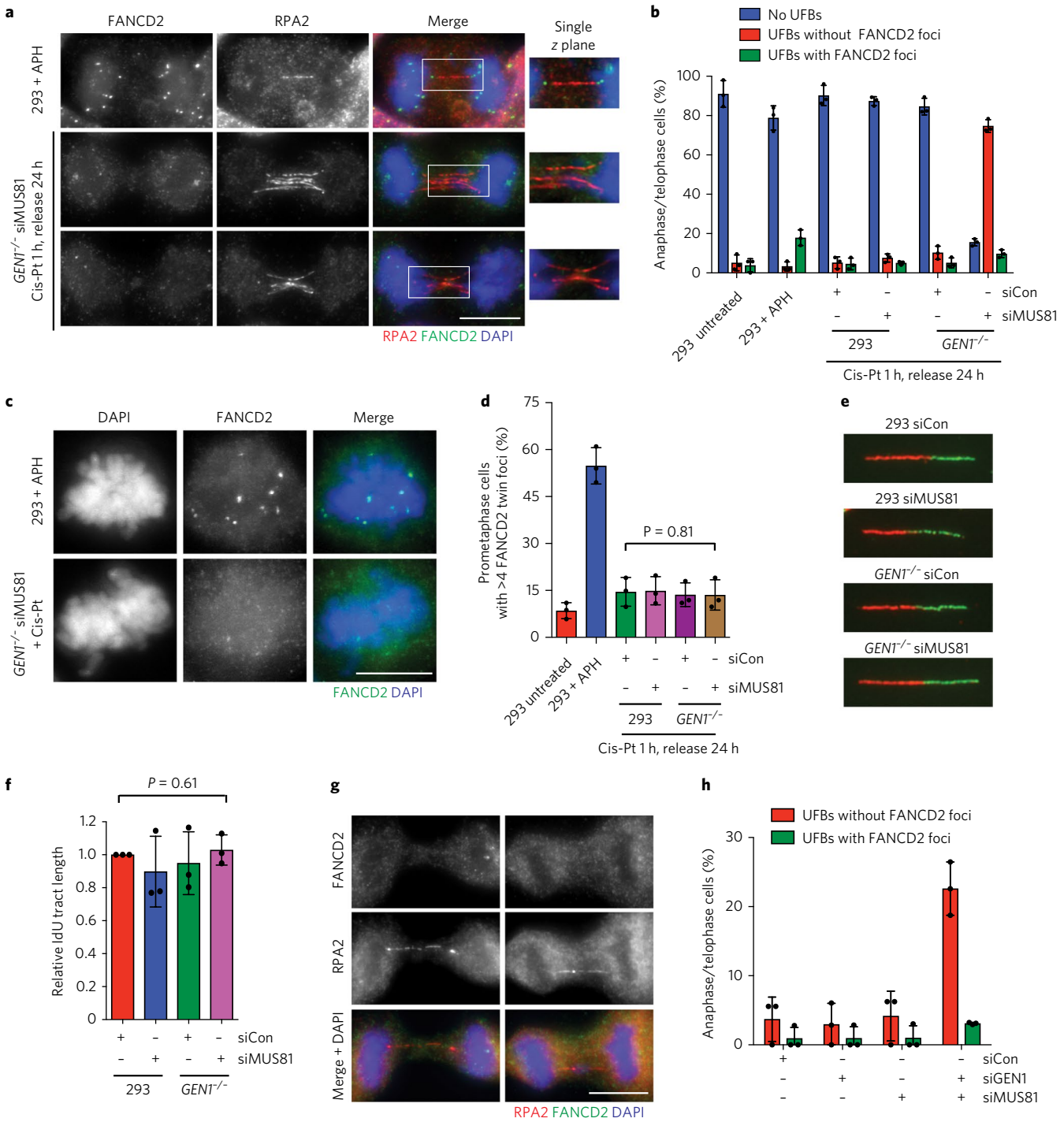

Fig. 2 | Persistent recombination intermediates lead to the formation of HR-UFBs. a, *GEN1*$^{-/-}$ cells were treated with control siRNA or siRNA against *MUS81* and with Cis-Pt for 1 h and released into fresh media for 24 h. Aphidicolin (APH)-treated (0.2 μM for 16 h) 293 cells were used as a control. RPA2, FANCD2 and DNA were visualized using anti-RPA2 antibody (red), anti-FANCD2 antibody (green) and DAPI (blue), respectively. Deconvoluted images are shown. Boxed regions are enlarged and single *z* planes are shown on the right. **b**, Quantification of cells with RPA2-positive UFBs (150 cells per condition) in anaphase/telophase, with or without FANCD2 foci, as visualized in **a**. **c**, Cells were treated as in **a**, and FANCD2 and DNA were visualized using anti-FANCD2 antibody (green) and DAPI (blue), respectively. Deconvoluted images are shown. **d**, Quantification of prometaphase cells with >4 FANCD2 twin foci (150 cells per condition) as visualized in **c**. **e**, *GEN1*$^{-/-}$ cells and 293 cells were treated with control siRNA or siRNA against *MUS81* for 48 h and then labelled with CldU and IdU for DNA fibre analysis. Representative fibres are shown. **f**, Quantification of IdU track length relative to 293 control cells (>200 fibres per condition) as in **e**. **g**, Representative images of hTERT-RPE1 cells treated with siRNAs against *GEN1* and *MUS81* and with Cis-Pt for 1 h and released into fresh media for 24 h. RPA2, FANCD2 and DNA were visualized using anti-RPA2 antibody (red), anti-FANCD2 antibody (green) and DAPI (blue), respectively. **h**, Quantification of hTERT-RPE1 cells in anaphase/telophase treated with control siRNA, siRNA against *GEN1* and/or *MUS81* and with Cis-Pt. Cells with RPA2-UFBs were classified as with or without FANCD2 foci (>100 cells per condition). In **a**, **c**, **e** and **g**, representative images of three independent experiments are shown. Quantified data in **b**, **d**, **f** and **h** represent the mean ± s.d. of $n = 3$ independent experiments. Source data are available in Supplementary Table 1. *P* values were determined using a two-tailed *t*-test. Scale bars, 10 μm.

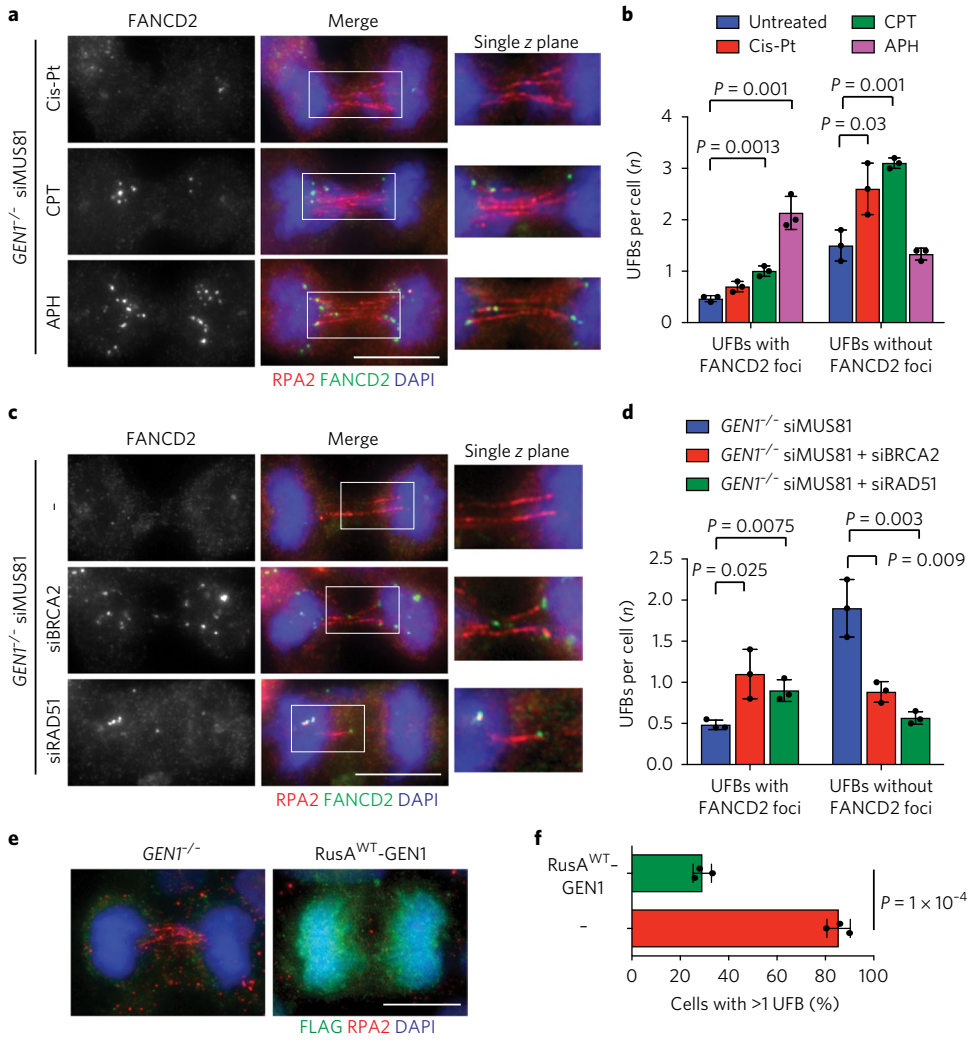

Fig. 3 | Generation of UFBs by homologous recombination in resolvase-deficient cells. a, *GEN1*$^{-/-}$ cells were treated with siRNA against *MUS81*. Cells were then either untreated or treated with Cis-Pt (1 μM for 1 h and released into fresh media for 24 h), camptothecin (CPT; 1 μM for 1 h and released for 24 h) or APH (0.2 μM for 16 h). RPA2, FANCD2 and DNA were visualized as indicated. Deconvoluted images are shown. Boxed regions are enlarged and single *z* planes are shown on the right. **b**, Quantification of anaphase/telophase cells (30 cells per condition) with RPA2-positive UFBs, classified as with or without FANCD2 foci, as visualized in **a**. **c**, *GEN1*$^{-/-}$ cells were treated with siRNA against *MUS81* alone or together with siRNA against *BRCA2* or *RAD51* for 72 h. RPA2, FANCD2 and DNA were visualized as indicated. Deconvoluted images are shown. Boxed regions are enlarged and single *z* planes are shown on the right. **d**, Quantification of anaphase/telophase cells (60 cells per condition) with RPA2-positive UFBs, classified as with or without FANCD2 foci, as visualized in **c**. **e**, *GEN1*$^{-/-}$ cells and *GEN1*$^{-/-}$ cells stably expressing RusA^{WT}-GEN1 were treated with siRNA against *MUS81* and with Cis-Pt. RPA2, RusA^{WT}-GEN1 and DNA were visualized using anti-RPA2 antibody (red), anti-FLAG antibody (green) and DAPI (blue), respectively. Deconvoluted images are shown. **f**, Quantification of cells (>150 cells per condition) with RPA2-positive UFBs as visualized in **e**. In **a**, **c** and **e**, representative images of three independent experiments are shown. Quantified data in **b**, **d** and **f** represent the mean ± s.d. of $n = 3$ independent experiments. Source data are available in Supplementary Table 1. *P* values were determined using a two-tailed *t*-test. Scale bars, 10 μm.

G1 phase (cyclin A-negative cells) by visualizing MDC1 foci (Fig. 4a,b). The number of MDC1 foci was significantly increased[38,39], and DNA damage was dependent on cell division. That is, treatment with nocodazole and the MPS1 inhibitor reversine, which inhibit spindle assembly and the mitotic checkpoint respectively, rescued the increased number of MDC1 foci (Fig. 4a,b). We also detected increased levels of cell division-dependent DNA breaks in the resolvase-deficient cells using alkaline comet assays (Supplementary Fig. 5b,c). In contrast, aphidicolin-induced G1 MDC1 foci were not affected by nocodazole and reversine treatment (Supplementary Fig. 5d,e), consistent with previous studies showing that replication stress-induced G1 lesions are transmitted from early mitosis to daughter cells rather than being generated by cell division[38].

To determine whether DNA damage, generated by breakage of the RPA-coated bridges, leads to cell cycle arrest (Fig. 1b), BrdU-pulse chase experiments were performed. Cells were briefly exposed to cisplatin for 1 h and the cells analysed for their DNA content 12–48 h after release (Fig. 4c). The resolvase-deficient cells displayed G2 arrest only in the second cell cycle (that is, 48 h after cisplatin release). These results contrast with those obtained after depletion of ERCC1, which is involved in the early stages of interstrand crosslink (ICL) unhooking[40,41], as ERCC1-depleted cells show pronounced G2 arrest 24 h after cisplatin release (that is, in the first cell cycle) (Supplementary Fig. 5f,g). Moreover, resolvase-deficient cells showed high levels of γH2AX, and phosphorylation of the ATM targets CHK2 T68 and KAP-1 S842, 48 h after drug release, correlating with the G2/M transition block

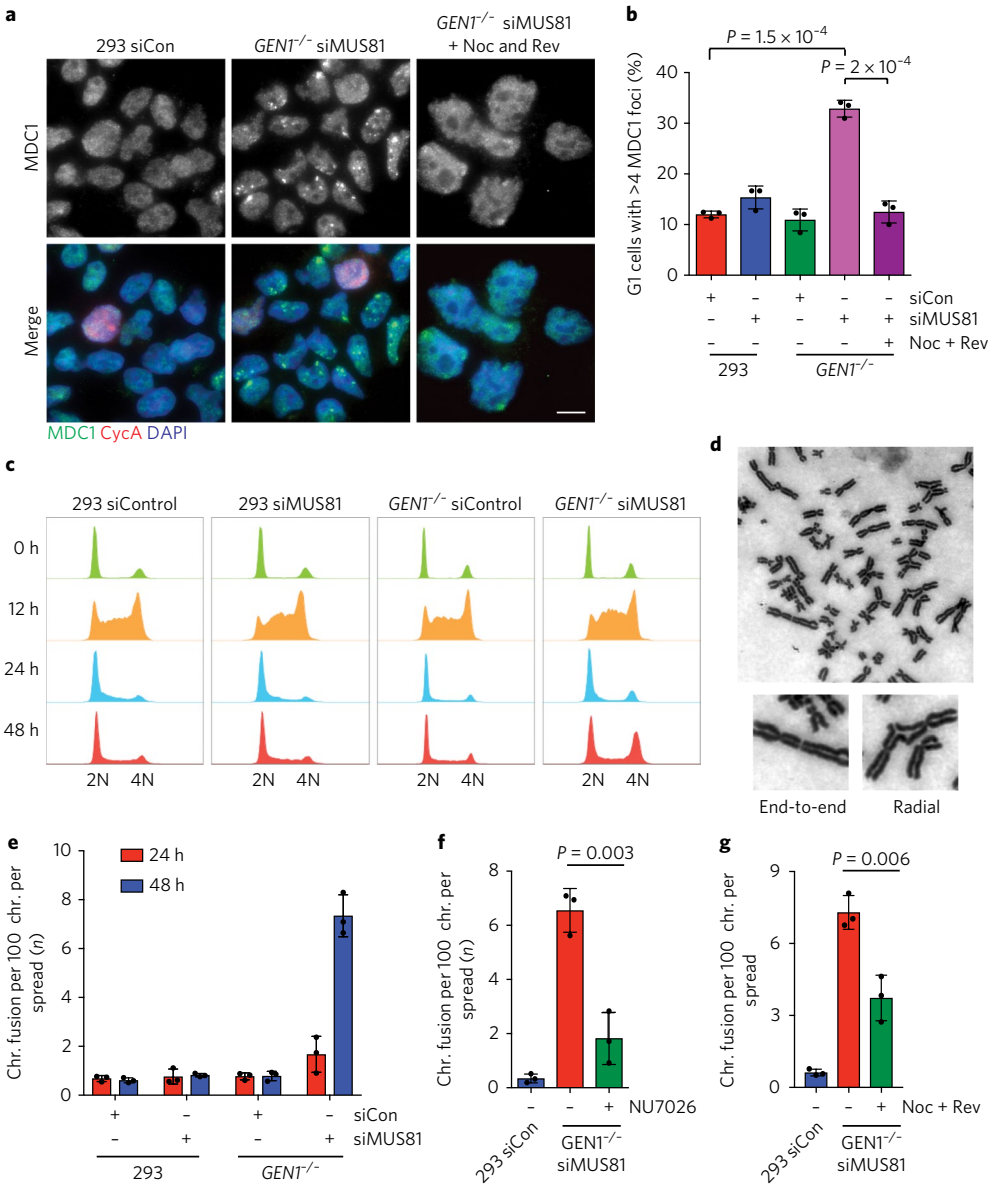

Fig. 4 | HR-UFB breakage leads to DNA damage and gross chromosome abnormalities. a, *GEN1*$^{-/-}$ cells and 293 cells were treated with control siRNA or siRNA against *MUS81* and with Cis-Pt and released into fresh media with or without nocodazole (Noc; 100 ng ml^{-1}) and reversine (Rev; 0.5 μM) for 24 h. MDC1, cyclin A (CycA) and DNA were visualized using anti-MDC1 antibody (green), anti-CycA antibody (red) and DAPI (blue), respectively. Scale bar, 10 μm. **b**, Quantification of G1 cells (>400 cells per condition) with > 4 MDC1 foci as in **a**. **c**, *GEN1*$^{-/-}$ cells and 293 cells were treated with control siRNA or siRNA against *MUS81* followed by Cis-Pt (1 μg ml^{-1}) and BrdU (10 μM) for 1 h. Cells were released into fresh media, collected at the indicated time points and analysed by FACS. The DNA content histograms of BrdU-negative mock-depleted 293 cells, MUS81-depleted 293 cells, mock-depleted *GEN1*$^{-/-}$ cells and MUS81-depleted *GEN1*$^{-/-}$ cells at the indicated time points are shown. **d**, Representative images of metaphase spreads from *GEN1*$^{-/-}$ cells treated with siRNA against *MUS81* and Cis-Pt and released into fresh media for 48 h. Representative end-to-end fusions and radials are shown. **e**, *GEN1*$^{-/-}$ cells and 293 cells were treated as in **d** but released into fresh media for 24 h (red) or 48 h (blue), and 75 metaphase spreads per condition were analysed for chromosome fusions in three independent experiments. **f**, *GEN1*$^{-/-}$ cells were treated as in **d**, except that DMSO or the DNA protein kinase inhibitor NU7026 (10 μM) was added 24 h before collection. Control siRNA-treated 293 cells were used as control. A total of 60 metaphase spreads per condition were analysed for chromosome fusions. **g**, Cells were treated as in **f** except Noc and Rev were added to the cells instead of NU7026. A total of 45 metaphase spreads per condition were analysed in three independent experiments. In **a** and **d**, representative images of three independent experiments are shown. Quantified data in **b** and **e**–**g** represent the mean ± s.d. of $n = 3$ independent experiments. Source data are available in Supplementary Table 1. *P* values were determined using a two-tailed *t*-test

(Supplementary Fig. 5h). CHK1 pS317 phosphorylation in response to ATR activation was not observed, indicating that cell cycle arrest was induced by DNA breaks rather than by replication checkpoint activation. Furthermore, inhibition of cell division by nocodazole and reversine treatment, which generated tetraploid cells with 8N DNA content, prevented activation of the DNA damage response, as measured by a reduction in S10 phosphorylation of histone H3 (Supplementary Fig. 6a–c). These results show that HR-UFB breakage is a consequence of cell division, leading to DNA damage in the subsequent cell cycle.

Analysis of metaphase spreads from control and resolvase-deficient cells (24 or 48 h after release from cisplatin treatment) revealed that resolvase-deficient cells exhibited an increased frequency of chromosome fusions (end-to-end fusions and radial chromosomes) after approximately two cell cycles (Fig. 4d,e). Inhibition of non-homologous end joining (NHEJ) by NU7026, a DNA-dependent protein kinase catalytic subunit inhibitor, suppressed this fusion phenotype (Fig. 4f). Blocking cell division by nocodazole and reversine treatment also partially rescued the increased frequency of chromosome fusions (Fig. 4g). Low levels of fusions also occurred in untreated resolvase-deficient cells (Supplementary Fig. 6d).

Resolvase-deficient cells also displayed an increased frequency of mis-segregation events compared with control cells (Supplementary Fig. 6e,f). Twenty-four hours after release from cisplatin, before chromosome fusions were prominent (Fig. 4e), most DAPI-positive anaphase bridges in the resolvase-deficient cells did not contain centromeres, indicating that they were induced by pre-mitotic defects[42]. After 48 h, the resolvase-deficient cells displayed an increased frequency of lagging chromosomes with centromeres, which correlates with chromosome fusions (Fig. 4d,e). Inhibition of NHEJ by NU7026 partially rescued the increased frequency of lagging chromosomes with centromeres (Supplementary Fig. 6g). These results show that HR-UFB breakage leads to gross chromosome abnormalities mediated through NHEJ-mediated chromosome fusions.

PICH and BLM promote ssDNA formation at UFBs. To understand how RPA-coated UFBs are generated from unresolved recombination intermediates, the bridges were stained using antibodies against BLM or PICH, a protein required for the recruitment of BLM[3,4,43] and RPA2 (Fig. 5a–d). In early anaphase, most UFBs were coated with RPA, PICH and BLM. However, in late anaphase and early telophase, some UFBs were coated only with RPA. The UFBs were exclusively RPA2-coated at late telophase, indicating that that duplex DNA bridges are converted to ssDNA, and that PICH and BLM play a role in their processing.

To determine how single-stranded HR-UFBs arise, resolvase-deficient cells were depleted of various DNA nucleases (TREX1, MRE11, CTIP, DNA2 or EXO1) or helicases (BLM, WRN, RECQ1, RECQ4, RECQ5 or RTEL1) and then analysed for RPA-positive UFB formation. Remarkably, only BLM depletion led to significantly fewer RPA-positive UFBs (Fig. 5e–g and Supplementary Fig. 7a,b). We therefore generated cell lines expressing either GFP-tagged wild-type or catalytic-dead (BLM^{K695M}) versions of BLM, and treated them with siRNAs against *BLM* (targeting the 3′ UTR of *BLM* mRNA), *GEN1* and *MUS81* (Supplementary Fig. 7c). The GFP-BLM^{K695M}-expressing cells exhibited a significantly reduced frequency of RPA-positive UFBs compared with those expressing GFP-BLM^{WT} (Fig. 6a,b). Moreover, those expressing GFP-BLM^{K695M} showed an increased percentage of cells with UFBs that were persistently coated with BLM.

Consistent with a role for BLM in the processing of HR-UFBs, an increased frequency of PICH-positive UFBs was observed when resolvase-deficient cells were depleted of BLM (Fig. 6c,d). We therefore sought to knockout PICH to specifically investigate the mitotic functions of BLM because PICH does not play a part in the interphase actions of BLM during DNA replication and repair[8,43]. However, we were unable to produce a complete PICH knockout in the *GEN1*$^{-/-}$ 293 cell line. We therefore targeted three out of the four alleles of *PICH* (this cell line is referred to as *GEN1*$^{-/-}$ *PICH*$^{3/4}$), which resulted in reduced *PICH* expression (Supplementary Fig. 7d,e) and slow growth compared with *GEN1*$^{-/-}$ cells (doubling time of 30 h versus 22 h; Supplementary Fig. 7f). The resolvase-deficient *PICH*$^{3/4}$ cells exhibited a significantly lower frequency of RPA-positive UFBs (Fig. 6e), supporting the hypothesis that PICH recruits BLM to unwind duplex DNA present in the HR-UFBs to generate the ssDNA bridges.

An inability to convert double-stranded bridges into fragile single-stranded UFBs might be expected to lead to cytokinesis failure. We therefore analysed the DNA content of resolvase-deficient *PICH*$^{3/4}$ cells (Fig. 6f,g). We observed a significant increase in their tetraploid (8N) population compared with PICH-proficient cells, similar to previous reports showing that *PICH*$^{-/-}$ DT40 cells display increased polyploidy[8]. These results indicate that PICH and BLM generate the single-stranded bridges that facilitate cell division.

A general mechanism for UFB processing. As HR-UFBs and replication stress-induced FS-UFBs both exhibit RPA binding (Figs. 2a and 3a), we next determined whether ssDNA formation represents a common mechanism of UFB processing. Generation of catenane-dependent centromeric UFBs using the topoisomerase II inhibitor ICRF-193 (Fig. 7a–d) induced the conversion of many centromeric UFBs to ssDNA. There was a clear reduction in the number of RPA-coated centromeric UFBs following depletion of BLM (Fig. 7a,b) or in *PICH*$^{3/4}$ cells (Fig. 7c,d), as observed previously[44]. These results indicate that HR-UFBs, FS-UFBs and C-UFBs are processed by a common mechanism involving ssDNA formation and RPA binding to facilitate their subsequent breakage and repair.

Discussion

In this work, we described the generation of a resolvase-deficient model that can be used to follow the biological fate of unresolved recombination intermediates at mitosis. Homologous recombination intermediates fail to elicit a checkpoint response and therefore persist until mitosis and give rise to a distinct class of UFBs. PICH and BLM act on the interlinked sister chromatids, which are converted to RPA-coated ssDNA bridges. These HR-UFBs are distinct from replication stress-induced UFBs that are characteristically flanked by FANCD2 foci. However, our data indicate that HR-UFBs, FS-UFBs and C-UFBs all share some common aspects of processing that are necessary for their breakage and result in chromosome segregation and cell division. Disruption of ssDNA formation, via inactivation of the BLM helicase, leads to cytokinesis failure.

Breaking chromosomal DNA requires up to ~100 nN force[45], which is ~100 times greater than the spindle forces generated by kinetochore fibres (~1 nN)[46]. However, the force required to break a single covalent bond is 1–2 nN[47,48], making it plausible that single-stranded bridges may be sheared by the tensile forces generated by the spindle during mitosis. In contrast to the single-stranded UFBs visualized here at anaphase/telophase, dicentric or lagging chromosomes induce cleavage furrow regression[49,50] or become stabilized as chromatin bridges between daughter cells, and persist for several hours until ssDNA become apparent and breakage occurs[15,50].

Figure 7e shows a schematic for HR-UFB processing. PICH recruits BLM helicase to HR-UFBs so that BLM can unwind the duplex DNA into single strands that are subsequently broken to permit cell division. Our work shows that HR-UFBs, FS-UFBs and C-UFBs all become decorated with RPA, a process dependent on PICH and BLM, indicating that DNA unwinding by BLM provides a universal mechanism that facilitates bridge resolution or breakage. Whether the initial duplex bridge needs to be nicked to allow access by PICH and BLM, or whether the tensile force of the spindle generates sufficient force to overstretch and melt the DNA to allow binding by PICH and BLM binding, is currently unknown.

Bridge processing reduces the risk of cytokinesis failure. However, this process may occur at the expense of DNA damage and the potential for chromosomal aberrations in the subsequent cell cycle. Indeed, in our resolvase-deficient system, we observed high levels of NHEJ-dependent end-to-end chromosome fusions and radial chromosomes, together with an increased frequency of mis-segregation. As the fusions were not observed when cell division was blocked by nocodazole and reversine treatment, they appear to be products of breakage that occurred in the previous mitosis. The breakage and

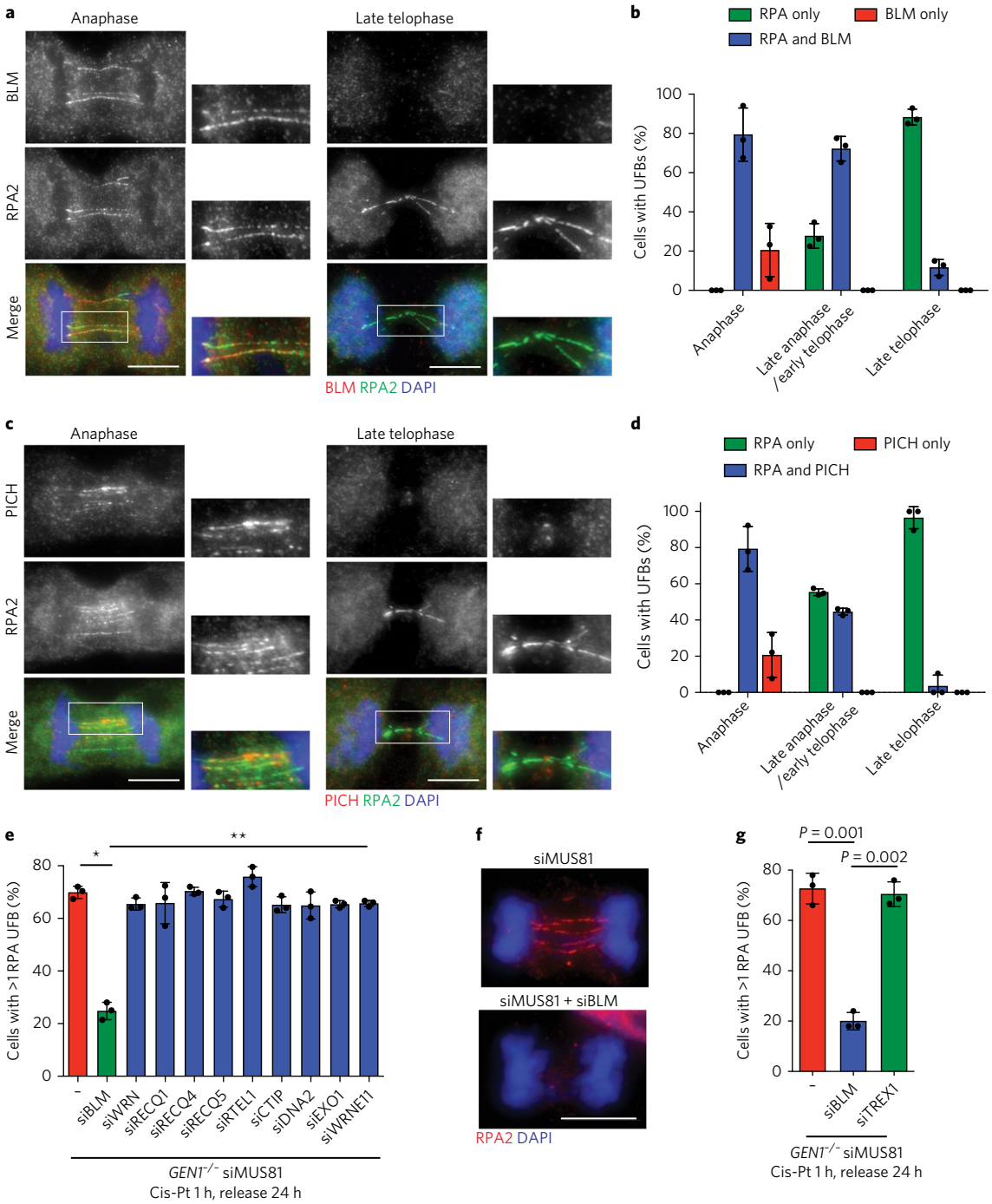

Fig. 5 | BLM is required for the formation of RPA-coated UFBs. a, U2OS cells were treated with siRNA against *GEN1* (siGEN1) and *MUS81* and with Cis-Pt and released into fresh media for 24 h. Cells with UFBs in different stages of mitosis were counted. BLM, RPA2 and DNA were visualized as indicated. Deconvoluted images are shown. Boxed regions are enlarged. **b**, Quantification of cells with UFBs (>250 cells counted) as in **a**. **c**, U2OS cells were treated as in **a**. PICH, RPA2 and DNA were visualized as indicated and deconvoluted images are shown. Boxed regions are enlarged. **d**, Quantification of cells with UFBs (>250 cells counted) as in **c**. **e**, *GEN1*$^{-/-}$ cells (–) (>150 cells per condition) were treated with siRNA against *MUS81* alone or together with the indicated siRNAs in which various nucleases or helicases were targeted and with Cis-Pt. The percentages of resolvase-deficient cells at anaphase/telophase with RPA2-positive UFBs were determined. **f**, *GEN1*$^{-/-}$ cells were treated with siRNA against *MUS81* alone or together with siRNA against *BLM* and with Cis-Pt. RPA2 and DNA were visualized as indicated. **g**, Quantification of anaphase/telophase cells (>150 cells per condition) with RPA2-positive UFBs. *GEN1*$^{-/-}$ cells (–) were treated with siRNA against *MUS81* alone or together with siRNA against *BLM* or *TREX1* and with Cis-Pt. In **a**, **c** and **f**, representative images of three independent experiments are shown. Quantified data in **b**, **d**, **e** and **g** represent the mean ± s.d. of $n = 3$ independent experiments. Source data are available in Supplementary Table 1. *P* values were determined using a two-tailed *t*-test, $^{*}P = 4 \times 10^{-5}$, $^{**}P < 0.002$. Scale bars, 10 μm.

reunion events observed here are consistent with previous studies showing that NHEJ promotes chromosome abnormalities such as translocations and chromothripsis following a defective mitosis[51,52].

Chromosomal instability (CIN) is a common trait of cancer cells. Cellular defects such as replication stress, merotelic kinetochore attachment and impairment of the cohesion network are

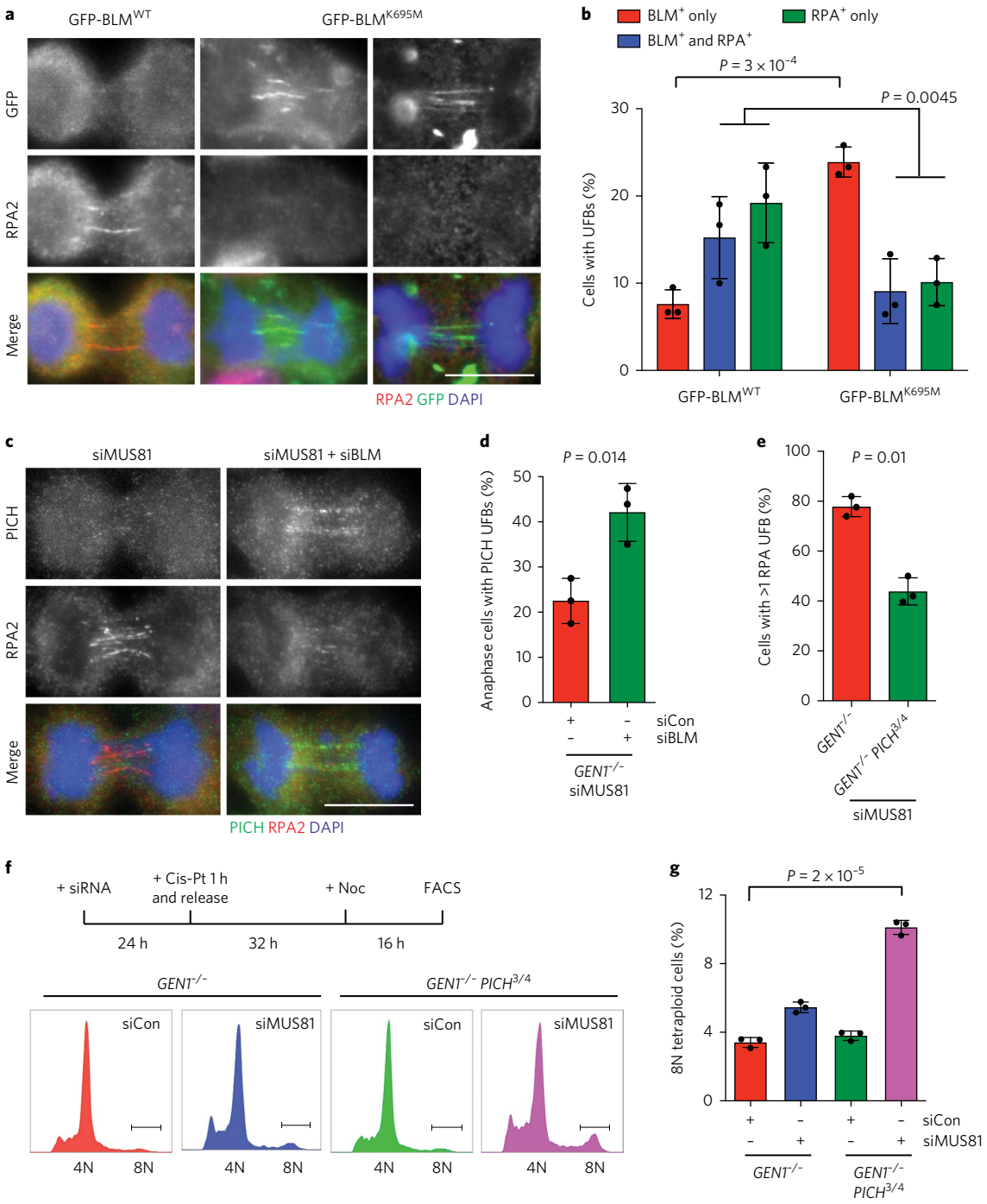

Fig. 6 | Unwinding of UFBs by PICH and BLM facilitates cell division. a, 293 cells stably expressing GFP-BLM^{WT} and GFP-BLM^{K695M} were treated with siRNAs against *GEN1*, *MUS81* and *BLM* and with Cis-Pt. RPA2, BLM and DNA were visualized using anti-RPA2 antibody (red), anti-GFP antibody (green) and DAPI (blue), respectively. **b**, Quantification of cells (>100 cells per condition) with UFBs shown in **a**. **c**, *GEN1*$^{-/-}$ cells were treated with siRNA against *MUS81* alone or together with siRNA against *BLM* and with Cis-Pt and then released into fresh media for 24 h. RPA2, PICH and DNA were visualized using anti-RPA2 antibody (red), anti-PICH antibody (green) and DAPI (blue), respectively. Deconvoluted images are shown. **d**, Quantification of anaphase cells with PICH-positive UFBs (>120 cells per condition) as visualized in **c**. **e**, *GEN1*$^{-/-}$ cells and *GEN1*$^{-/-}$ *PICH*$^{3/4}$ cells were treated with siRNA against *MUS81* and with Cis-Pt. The number of cells with RPA2-positive UFBs was quantified (>150 cells per condition). **f**, *GEN1*$^{-/-}$ and *GEN1*$^{-/-}$ *PICH*$^{3/4}$ cells were treated as shown in the scheme (upper panel), and their DNA content distributions were determined by FACS analysis (lower panel). **g**, The percentage of cells with 8N DNA content, as determined in **f**, was quantified. In **a**, **c** and **f**, representative data of three independent experiments are shown. Quantified data in **b**, **d**, **e** and **g** represent the mean ± s.d. of $n = 3$ independent experiments. Source data are available in Supplementary Table 1. *P* values were determined using a two-tailed *t*-test. Scale bars, 10 μm.

known to drive CIN[42,53,54]. Our findings reveal that unresolved recombination intermediates may also serve as a potential driver of CIN. Although resolvase deficiency has not yet been described in any cancer model, and our model system provides an extreme demonstration of the fate of multiple unresolved recombination intermediates, our results demonstrate the fate of any homologous

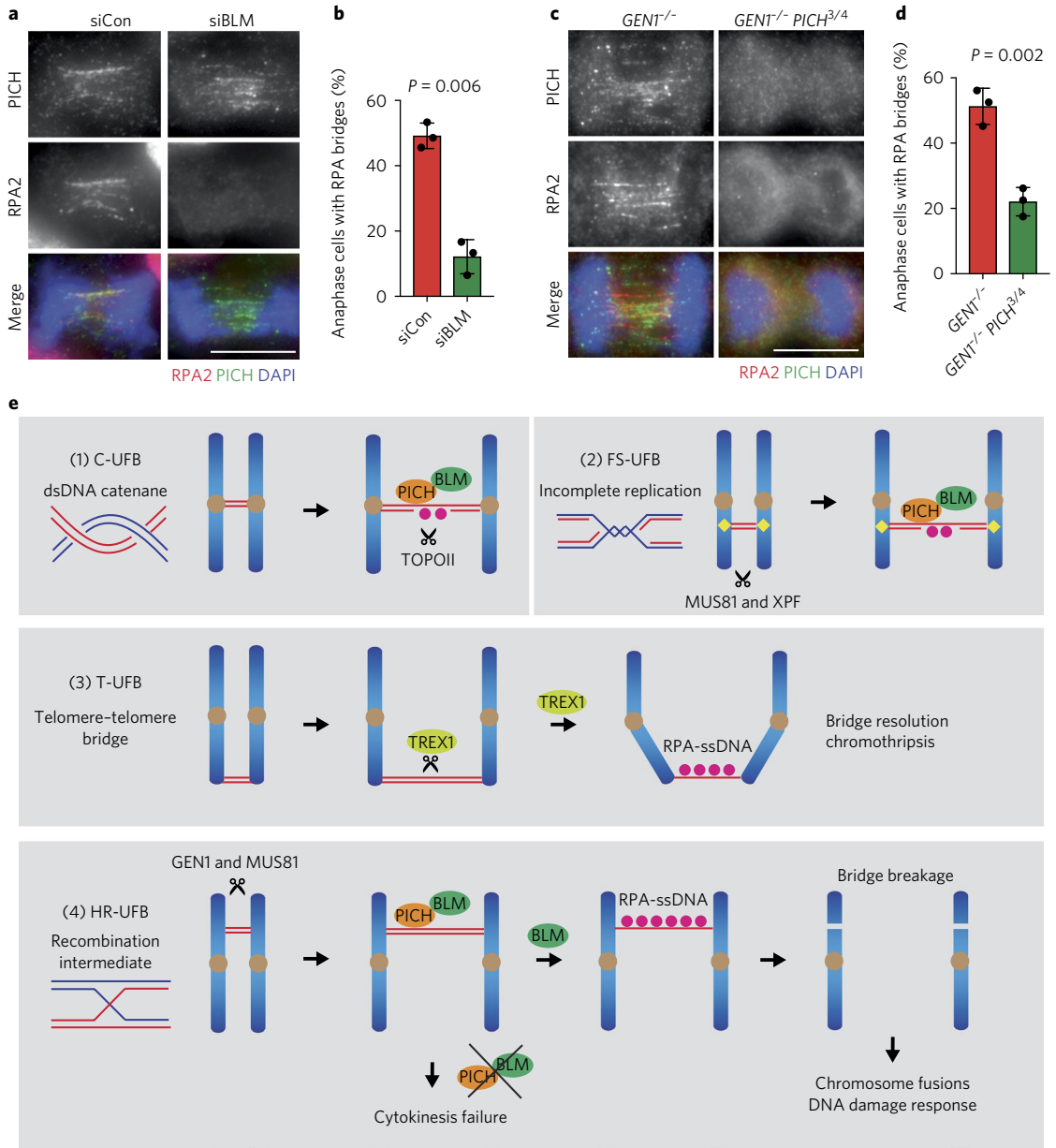

Fig. 7 | General mechanism for the formation of single-stranded UFBs. a, 293 cells were treated with control siRNA or siRNA against *BLM* and with ICRF-193 (0.1 μM for 1 h). PICH, RPA2 and DNA were visualized as indicated. **b**, Quantification of cells (>100 cells per condition) with RPA2-coated UFBs in **a**. **c**, *GEN1*$^{-/-}$ cells and *GEN1*$^{-/-}$ *PICH*$^{3/4}$ cells were treated with ICRF-193 (0.1 μM for 1 h). PICH, RPA2 and DNA were visualized as indicated. **d**, Quantification of cells (>120 cells per condition) with RPA2-coated UFBs in **c**. **e**, Schematic of the four types of anaphase UFBs. (1) C-UFBs emerge from centromeric regions, possess double-stranded catenanes and are resolved by PICH and BLM and topoisomerase II (TOPII). Recruitment of BLM is required for RPA formation. (2) FS-UFBs emerge from incompletely replicated DNA at CFSs (yellow rhombus) and are flanked by FANCD2 twin foci. The bridges frequently possess regions that are bound by RPA. (3) T-UFBs originate from telomere fusions, persist and develop into chromatin bridges that are processed by TREX1 to ultimately generate ssDNA. (4) HR-UFBs originate from unresolved recombination intermediates. In the absence of GEN1 and MUS81, HR-UFBs accumulate at anaphase, and PICH and BLM are recruited for DNA unwinding, ssDNA formation and breakage at mitosis. See main text for further details. In **a** and **c**, representative images of three independent experiments are shown. Quantified data in **b** and **d** represent the mean ± s.d. of $n = 3$ independent experiments. Source data are available in Supplementary Table 1. *P* values were determined using a two-tailed *t*-test. Scale bars, 10 μm.

recombination intermediates that escape detection by the dissolution and resolution pathways. These findings may be particularly pertinent to cancer cells in which the homologous recombination pathway is hyper-activated and the load of recombination intermediates is increased (for example, when RAD51 activity is increased)[55–57]. Finally, the synthetic lethal relationship observed between MUS81 and SLX4 and GEN1 indicates that resolvases might represent plausible targets for cancer therapies, possibly in combination with DNA-damaging agents such as cisplatin. It may therefore be interesting to determine whether tumours that confer resistance to DNA-damaging agents due to enhanced homologous recombination-mediated repair show a selective sensitivity to resolvase inhibition compared with normal cells.

Methods

Methods, including statements of data availability and any associated accession codes and references, are available at https://doi.org/10.1038/s41556-017-0011-1.

Received: 28 March 2017; Accepted: 16 November 2017;
Published online: 18 December 2017

References

1. Uhlmann, F. SMC complexes: from DNA to chromosomes. *Nat. Rev. Mol. Cell Biol.* **17**, 399–412 (2016).
2. Chan, K. L. & Hickson, I. D. New insights into the formation and resolution of ultra-fine anaphase bridges. *Sem. Cell Dev. Biol.* **22**, 906–912 (2011).
3. Baumann, C., Korner, R., Hofmann, K. & Nigg, E. A. PICH, a centromere-associated SNF2 family ATPase, is regulated by PLK1 and required for the spindle checkpoint. *Cell* **128**, 101–114 (2007).
4. Chan, K. L., North, P. S. & Hickson, I. D. BLM is required for faithful chromosome segregation and its localization defines a class of ultrafine anaphase bridges. *EMBO J.* **26**, 3397–3409 (2007).
5. Chan, K. L. & Hickson, I. D. On the origins of ultra-fine anaphase bridges. *Cell Cycle* **8**, 3065–3066 (2009).
6. Germann, S. M. et al. TopBP1/Dpb11 binds DNA anaphase bridges to prevent genome instability. *J. Cell Biol.* **204**, 45–59 (2014).
7. Liu, Y., Nielsen, C. F., Yao, Q. & Hickson, I. D. The origins and processing of ultra fine anaphase DNA bridges. *Curr. Opin. Genet. Dev.* **26**, 1–5 (2014).
8. Nielsen, C. F. et al. PICH promotes sister chromatid disjunction and co-operates with topoisomerase II in mitosis. *Nat. Commun.* **6**, 8962 (2015).
9. Wang, L. H., Schwarzbam, T., Speicher, M. R. & Nigg, E. A. Persistence of DNA threads in human anaphase cells suggests late completion of sister chromatid decatenation. *Chromosoma* **117**, 123–135 (2008).
10. Chan, K. L., Palmai-Pallag, T., Ying, S. M. & Hickson, I. D. Replication stress induces sister-chromatid bridging at fragile site loci in mitosis. *Nat. Cell Biol.* **11**, 753–760 (2009).
11. Naim, V. & Rosselli, F. The FANC pathway and BLM collaborate during mitosis to prevent micro-nucleation and chromosome abnormalities. *Nat. Cell Biol.* **11**, 761–768 (2009).
12. Naim, V., Wilhelm, T., Debatisse, M. & Rosselli, F. ERCC1 and MUS81-EME1 promote sister chromatid separation by processing late replication intermediates at common fragile sites during mitosis. *Nat. Cell Biol.* **15**, 1008–1015 (2013).
13. Ying, S. M. et al. MUS81 promotes common fragile site expression. *Nat. Cell Biol.* **15**, 1001–1007 (2013).
14. Barefield, C. & Karlseder, J. The BLM helicase contributes to telomere maintenance through processing of late-replicating intermediate structures. *Nucl. Acids Res.* **40**, 7358–7367 (2012).
15. Maciejowski, J., Li, Y., Bosco, N., Campbell, P. J. & de Lange, T. Chromothripsis and kataegis induced by telomere crisis. *Cell* **163**, 1641–1654 (2015).
16. Nera, B., Huang, H.-S., Lai, T. & Xu, L. X. Elevated levels of TRF2 induce telomeric ultrafine anaphase bridges and rapid telomere deletions. *Nat. Commun.* **6**, 10132 (2015).
17. Sarbajna, S., Davies, D. & West, S. C. Roles of SLX1-SLX4, MUS81-EME1 and GEN1 in avoiding genome instability and mitotic catastrophe. *Genes Dev.* **28**, 1124–1136 (2014).
18. Wu, L. & Hickson, I. D. The Bloom's syndrome helicase suppresses crossing over during homologous recombination. *Nature* **426**, 870–874 (2003).
19. Chen, X. B. et al. Human MUS81-associated endonuclease cleaves Holliday junctions in vitro. *Mol. Cell* **8**, 1117–1127 (2001).
20. Ciccia, A., Constantinou, A. & West, S. C. Identification and characterization of the human MUS81/EME1 endonuclease. *J. Biol. Chem.* **278**, 25172–25178 (2003).
21. Fekairi, S. et al. Human SLX4 is a Holliday junction resolvase subunit that binds multiple DNA repair/recombination endonucleases. *Cell* **138**, 78–89 (2009).
22. Munoz, I. M. et al. Coordination of structure-specific nucleases by human SLX4/BTBD12 is required for DNA repair. *Mol. Cell* **35**, 116–127 (2009).
23. Svendsen, J. M. et al. Mammalian BTBD12/SLX4 assembles a Holliday junction resolvase and is required for DNA repair. *Cell* **138**, 63–77 (2009).
24. Ip, S. C. Y. et al. Identification of Holliday junction resolvases from humans and yeast. *Nature* **456**, 357–361 (2008).
25. Rass, U. et al. Mechanism of Holliday junction resolution by the human GEN1 protein. *Genes Dev.* **24**, 1559–1569 (2010).
26. Chan, Y. W. & West, S. C. GEN1 promotes Holliday junction resolution by a coordinated nick and counter-nick mechanism. *Nucl. Acids Res.* **43**, 10882–10892 (2015).
27. Wyatt, H. D. M., Laister, R. C., Martin, S. R., Arrowsmith, C. H. & West, S. C. The SMX DNA repair tri-nuclease. *Mol. Cell* **65**, 848–860 (2017).
28. Wyatt, H. D. M., Sarbajna, S., Matos, J. & West, S. C. Coordinated actions of SLX1-SLX4 and MUS81-EME1 for Holliday junction resolution in human cells. *Mol. Cell* **52**, 234–247 (2013).
29. Wechsler, T., Newman, S. & West, S. C. Aberrant chromosome morphology in human cells defective for Holliday junction resolution. *Nature* **471**, 642–646 (2011).
30. Castor, D. et al. Cooperative control of Holliday junction resolution and DNA repair by the SLX1 and MUS81-EME1 nucleases. *Mol. Cell* **52**, 221–233 (2013).
31. Garner, E., Kim, Y., Lach, F. P., Kottemann, M. C. & Smogorzewska, A. Human GEN1 and the SLX4-associated nucleases MUS81 and SLX1 are essential for the resolution of replication-induced Holliday junctions. *Cell Rep.* **5**, 207–215 (2013).
32. Duda, H. et al. A mechanism for controlled breakage of under-replicated chromosomes during mitosis. *Dev. Cell* **39**, 740–755 (2016).
33. Matos, J., Blanco, M. G., Maslen, S. L., Skehel, J. M. & West, S. C. Regulatory control of the resolution of DNA recombination intermediates during meiosis and mitosis. *Cell* **147**, 158–172 (2011).
34. Chan, Y. W. & West, S. C. Spatial control of the GEN1 Holliday junction resolvase ensures genome stability. *Nat. Commun.* **5**, 5844 (2014).
35. Nair, N., Castor, D., Macartney, T. & Rouse, J. Identification and characterization of MUS81 point mutations that abolish interaction with the SLX4 scaffold protein. *DNA Rep.* **24**, 131–137 (2014).
36. Minocherhomji, S. et al. Replication stress activates DNA repair synthesis in mitosis. *Nature* **528**, 286–290 (2015).
37. Schlacher, K. et al. Double-strand break repair-independent role for BRCA2 in blocking stalled replication fork degradation by MRE11. *Cell* **145**, 529–542 (2011).
38. Lukas, C. et al. 53BP1 nuclear bodies form around DNA lesions generated by mitotic transmission of chromosomes under replication stress. *Nat. Cell Biol.* **13**, 243–253 (2011).
39. Harrigan, J. A. et al. Replication stress induces 53BP1-containing OPT domains in G1 cells. *J. Cell Biol.* **193**, 97–108 (2011).
40. Klein Douwel, D. et al. XPF-ERCC1 acts in unhooking DNA interstrand crosslinks in cooperation with FANCD2 and FANCP/SLX4. *Mol. Cell* **54**, 460–471 (2014).
41. Hodskinson, M. R. G. et al. Mouse SLX4 is a tumour suppressor that stimulates the activity of the nuclease XPF-ERCC1 in DNA crosslink repair. *Mol. Cell* **54**, 472–484 (2014).
42. Burrell, R. A. et al. Replication stress links structural and numerical cancer chromosomal instability. *Nature* **494**, 492–496 (2013).
43. Ke, Y. et al. PICH and BLM limit histone association with anaphase centromeric threads and promote their resolution. *EMBO J.* **30**, 3309–3321 (2011).
44. Hengeveld, R. C. et al. Rif1 Is required for resolution of ultrafine DNA bridges in anaphase to ensure genomic stability. *Dev. Cell* **34**, 466–474 (2015).
45. Houchmandzadeh, B., Marko, J. F., Chatenay, D. & Libchaber, A. Elasticity and structure of eukaryote chromosomes studied by micromanipulation and micropipette aspiration. *J. Cell Biol.* **139**, 1–12 (1997).
46. Alexander, S. P. & Rieder, C. L. Chromosome motion during attachment to the vertebrate spindle: initial saltatory-like behavior of chromosomes and quantitative analysis of force production by nascent kinetochore fibers. *J. Cell Biol.* **113**, 805–815 (1991).
47. Grandbois, M., Beyer, M., Rief, M., Clausen-Schaumann, H. & Gaub, H. E. How strong is a covalent bond? *Science* **283**, 1727–1730 (1999).
48. Bustamante, C., Smith, S. B., Liphardt, J. & Smith, D. R. Single-molecule studies of DNA molecules. *Curr. Opin. Struct. Biol.* **10**, 279–285 (2000).
49. Mullins, J. M. & Biesele, J. J. Terminal phase of cytokinesis in D-98s cells. *J. Cell Biol.* **73**, 672–684 (1977).
50. Steigemann, P. et al. Aurora B-mediated abscission checkpoint protects against tetraploidization. *Cell* **136**, 473–484 (2009).
51. Janssen, A., van der Burg, M., Szuhai, K., Kops, G. J. & Medema, R. H. Chromosome segregation errors as a cause of DNA damage and structural chromosome aberrations. *Science* **333**, 1895–1898 (2011).
52. Ly, P. et al. Selective Y centromere inactivation triggers chromosome shattering in micronuclei and repair by non-homologous end joining. *Nat. Cell Biol.* **19**, 68–75 (2017).
53. Thompson, S. L. & Compton, D. A. Examining the link between chromosomal instability and aneuploidy in human cells. *J. Cell Biol.* **180**, 665–672 (2008).
54. Tanno, Y. et al. The inner centromere-shugoshin network prevents chromosomal instability. *Science* **349**, 1237–1240 (2015).
55. Raderschall, E. et al. Formation of higher-order nuclear RAD51 structures is functionally linked to p21 expression and protection from DNA damage-induced apoptosis. *J. Cell Sci.* **115**, 153–164 (2002).
56. Klein, H. L. The consequences of RAD51 overexpression for normal and tumor cells. *DNA Repair* **7**, 686–693 (2008).
57. Marsden, C. G. et al. The tumor-associated variant RAD51 G151D induces a hyper-recombination phenotype. *PLoS Genet.* **12**, e1006208 (2016).

Acknowledgements

We thank members of the West Lab for their help and encouragement, and K. L. Chan (University of Sussex, UK) for sharing unpublished data. This work was supported by the Francis Crick Institute (FC10212), the European Research Council (ERC-ADG-249145 and ERC-ADG-666400) and the Louis-Jeantet Foundation. The Francis Crick Institute receives core funding from Cancer Research UK, the Medical Research Council and the Wellcome Trust. K.F. is the recipient of a fellowship from the Lundbeck Foundation.

Author contribution

Y.W.C. carried out the experiments and was assisted by K.F with the fibre assays and some of the immunofluorescence experiments. Y.W.C. and S.C.W. designed the project and wrote the manuscript.

Competing interests

The authors have no competing financial interests.

Additional information

Supplementary information is available for this paper at https://doi.org/10.1038/s41556-017-0011-1.

Correspondence and requests for materials should be addressed to S.C.W.

Methods

Plasmids. GEN1 and GEN1^{EEAA} carrying 3xFLAG tags at their C termini were cloned into the pcDNA5/FRT/TO vector (Life Technologies) as previously described[34]. Plasmids encoding RusA^{WT} and RusA^{D70N} (pMW462 and pMW463) were kindly provided by Matthew Whitby (University of Oxford, UK)[58]. RusA^{WT} and RusA^{D70N} sequences were cloned into the N terminus of GEN1^{EEAA}-3xFLAG using an In-Fusion Cloning kit (Clontech). To generate the sgRNA vectors for gene targeting, pairs of annealed oligonucleotides (see below) were cloned into the pX330 or pX459 plasmids according to published protocols[59,60]. The pEGFP-C2 vector carrying GFP-BLM was a gift from Ian Hickson (University of Copenhagen, Denmark). The catalytic-dead mutant of BLM, BLM^{K695M}, was generated using a QuikChange Lightning Multi Site-Directed Mutagenesis kit (Agilent).

The following sequences of sgRNA oligonucleotides were used for gene targeting:

GEN1: 5′-CACCGCACATCCCCTTGCGTAATCT-3′ and
5′-AAACAGATTACGCAAGGGGATGTGC-3′; ref. [34]
MUS81: 5′-CACCGTCTGAAATACGAAGCGCGTG-3′ and
5′-AAACCACGCGCTTCGTATTTCAGAC-3′;
SLX1: 5′-CACCGTAGACGCCGAAAAAGCGCCC-3′ and
5′-AAACGGGCGCTTTTTCGGCGTCTAC-3′;
SLX4: 5′-CACCGCCGGTGCTGAAGAAGGAAC-3′ and
5′-AAACGTTCCTTCTTCAGCACCGGC-3′;
PICH: 5′-CACCGCCGAAGGTTTCCGGAAGCCG-3′ and
5′-AAACCGGCTTCCGGAAACCTTCGGC-3′. ref. [8]

Cell culture and transfection. Flp-In T-REx 293 cells (Thermo Fisher) and U2OS cells (ATCC) were cultured in DMEM medium (Life Technologies). eHAP cells (Horizon Discovery)[61] were cultured in IMDM medium (Life Technologies). hTERT-RPE1 cells (ATCC) were cultured in DMEM/F-12(1:1) medium (Life Technologies). All cells were grown at 37 °C in 5% CO_2. Cultures were supplemented with 10% fetal bovine serum and penicillin and streptomycin. Although initially haploid, the eHAP cell lines tend to stabilize their DNA content at the diploid level, as assayed by FACS; so, diploid clones were selected for all experiments for consistency. Geneticin (400 μg ml^{-1}), hygromycin (100 μg ml^{-1}), zeocin (50 μg ml^{-1}) and blasticidin (4 μg ml^{-1}) were obtained from Life Technologies. Nocodazole (100 ng ml^{-1}), cisplatin (as indicated), hydroxyurea (2 mM), reversine (0.5 μM), NU7026 (10 μM), ICRF-193 (0.1 μM) and BrdU (10 or 100 μM) were obtained from Sigma-Aldrich. To generate stable cell lines expressing the RusA and GEN1 proteins, Flp-In T-REx 293 cells were co-transfected with pcDNA5/FRT/TO plasmids encoding the protein of interest, together with the plasmid pOG44, which encodes Flp recombinase (1:9 ratio). Hygromycin-resistant colonies were picked and expanded. Protein expression was induced using tetracycline (10–50 ng ml^{-1}; Sigma-Aldrich). To generate stable cell lines expressing BLM, Flp-In T-REx 293 cells were transfected with pEGFP-C2 and geneticin-resistant colonies were picked and expanded. All cell lines used in this study were certified free of mycoplasma.

For gene targeting, cells were transfected with pX330 or PX459 carrying the targeting sequences, together with pSuper.puro (Oligoengine) at a 9:1 ratio. After 24–48 h, cells were selected with puromycin (2 μg ml^{-1}) and seeded as single colonies. Clones were picked and first selected on the basis of a negative signal when subjected to western blotting. The selected clones were then verified by sequencing. To this end, genomic DNA was extracted from cells with a DNeasy Blood & Tissue kit (Qiagen), and PCR was carried out using KOD Hot Start DNA Polymerase (Novagen) to amplify the targeted locus using a forward and a reverse primer (see below). The PCR product was then purified using a QIAquick PCR Purification kit (Qiagen) and finally sequenced. For genes that have more than two alleles in 293 cells, the PCR products were cloned into pJet vector using a CloneJET PCR Cloning kit (Thermo Fisher). The plasmids were then sequenced to identify mutations in all alleles. To generate endogenous mutations in *SLX4* (E1577A and L1578A), a single-stranded oligodeoxynucleotide template (5′-GTGCTAATCGGAAGAAGAACTTGCCCCCCAAAGTGCCCATAACGC CGATGCCACAGTATTCCATTATGGAGACGCCGGTGCTGAAGAAGGCA GCTGATAGGTTGGCGGTCTTCAAAGCTTGTTGCCCACAGTGGTCTTTT CCCTCCCATAAGTAACTGGGTTTCACACACCTGGGGGCGGAAGGGC-3′; Integrated DNA Technologies) was co-transfected (10 μL of 10 μM for a 60 mm plate) with the sgRNA vector.

The following primer sequences were used to verify gene targeting:
GEN1: 5′-GTGGCTTATAATATATTGTTTG-3′ and 5′-GCTTTTAGTATCTG AAGCATC-3′; *MUS81*: 5′-GAATCCCGACTCCAGAACTG-3′ and 5′-GCTCGTCCAGCATCCGGCAG-3′; *SLX1*: 5′ -GAGCTTGTTCCGAAGCAAGC-3′ and 5′-CGTGCACGACGAGCACCATC-3′; *SLX4*: 5′-TTACCCAGAAGGTGCTAATCG-3′ and 5′ -GCCTGGTGTGGTGGCGTGTGC-3′; *PICH*: 5′ -GGAGTGAGCGAAATTCAAGC-3′ and 5′-AGACTTAGGGCTTGATAAGC-3′.

Cell extracts, immunoprecipitation and western blotting. Cell lysates were prepared by resuspending cells in HEPES lysis buffer (50 mM HEPES pH 7.4, 150 mM NaCl, 0.1% Triton X-100, 10% glycerol, 1 mM dithiothreitol) supplemented with protease and phosphatase inhibitors. The lysates were incubated on ice for 30 min and then cleared by centrifugation (14,000 r.p.m. for 30 min in an Eppendorf 5430R). For immunoprecipitation, 0.5 μg of antibody was incubated with 0.5 mg of cleared lysate, and protein was affinity purified using protein G sepharose (GE Healthcare). The beads were then washed extensively with lysis buffer and analysed by western blotting. For western blotting of BRCA2 and RAD51, RIPA buffer (50 mM Tris-HCl pH 7.5, 150 mM NaCl, 1% Triton X-100, 0.5% sodium deoxycholate, 0.1% SDS and 5 mM EDTA) was used to lyse the cells.

Proteins were detected by western blotting using the following primary antibodies: rabbit anti-MRE11 (1:1000; Cell Signaling 48955); rabbit anti-DNA2 (1:1000; Abcam ab96488); rabbit anti-EXO1 (1:1000; Abcam ab95068); rabbit anti-CTIP (1:1000; Bethyl Laboratories A300-488A); rabbit anti-RTEL1 (1:1000; Novus Biologicals NBP2-22360); rabbit anti-RECQ1 (1:1000; Bethyl Laboratories A300-447A); rabbit anti-RAD51 (1:200; Santa Cruz Biotechnology sc-8349); mouse anti-BRCA2 (1:1000; Calbiochem OP95); mouse anti-α-tubulin (1:5000; Sigma T9026); mouse anti-FLAG HRP (1:1000; Sigma-Aldrich A8592); mouse anti-MUS81 (1:1000; Santa Cruz Biotechnology sc-47692); rabbit anti-BLM (1:1000; Abcam ab2179); rabbit anti-KAP-1 pSer842 (1:1000; Abcam ab70369); mouse-anti-CHK1 (1:1000; Sigma-Aldrich C9358); rabbit anti-CHK1 pSer317 (1:1000; Cell Signaling 2341); mouse anti-histone H2A.X pSer139 (1:1000; Millipore 05-636-1); mouse anti-CHK2 (1:1000; Millipore 05-649); rabbit anti-CHK2 pThr68 (1:1000; Cell Signaling 2661); mouse anti-RPA2 (1:1000; Abcam ab2175); rabbit anti-ERCC1 (1:200; Santa Cruz Biotechnology sc-10785); mouse anti-PICH (1:500; Millipore 04-1540); rabbit anti-GEN1 (1:100; raised against GEN1$^{890\text{-}908}$)[25]; sheep anti-SLX1 and sheep anti-SLX4 (1:500; gifts from John Rouse, Dundee University); rabbit anti-WRN, rabbit anti-RECQ4 and rabbit anti-RECQ5 (1:500; gifts from Pavel Janscak, University of Zurich). For Supplementary Figs. 3k, 4f,g and 7a, primary antibody detection was performed using IRDye 680RD/800CW-conjugated donkey anti-mouse or anti-rabbit antibodies (LI-COR) and a LI-COR Odyssey CLx imaging system. For all the other western blot analyses, primary antibody detection was performed using HRP-conjugated goat anti-mouse or anti-rabbit antibodies (Dako), or HRP-conjugated rabbit anti-sheep antibody (Abcam) and exposure to Amersham Hyperfilm ECL film (GE Healthcare).

Immunofluorescence and EdU labelling. For immunofluorescence analyses, cells grown on coverslips were fixed with PTEMF buffer (20 mM PIPES pH 6.8, 0.2% Triton X-100, 1 mM $MgCl_2$, 10 mM EGTA and 4% paraformaldehyde) for 10 min. Cells were then permeabilized with 0.2% Triton X-100 in PBS for 5 min and blocked with 3% BSA in PBS for 30 min. Cells were incubated with primary antibodies diluted in 3% BSA in PBS for 1 h, washed with PBS and incubated with secondary antibodies diluted in 3% BSA in PBS for 1 h. The coverslips were washed twice with PBS and then mounted with Prolong Diamond antifade mountant (Thermo Fisher). The following primary antibodies were used: rabbit anti-GFP (1:5000; Abcam ab290); mouse anti-cyclin A (1:200; Santa Cruz Biotechnology sc-56299); rabbit anti-MDC1 (1:1000; Abcam ab11169); mouse anti-RPA2 (1:1000; Abcam ab2175); rabbit anti-RPA2 (1:1000; Abcam ab97594); mouse anti-FLAG (1:1000; Sigma-Aldrich A8592); rabbit anti-BLM (1:1000; Abcam ab 2179); rabbit anti-FANCD2 (1:1000; Novus Biologicals NB100-182); human anti-centromere CREST (1:1000; Immunovision HCT-0100); rabbit anti-PICH (1:100; Cell Signaling 8886); rabbit anti-TREX1 (1:1000; Abcam ab185288); rabbit anti-MKLP1 (1:1000; Santa Cruz Biotechnology sc-867). Secondary antibodies conjugated to Alexa Fluor 488, Alexa Fluor 555 and Alexa Fluor 647 (1:2000; Thermo Fisher) were used for detection. DNA was stained with DAPI. Images were acquired using a Zeiss AXIO Imager M2 microscope with a plan-SPOCHROMAT 63×1.4 oil objective (Zeiss) and Hamamatsu photonics camera under the control of Volocity software (PerkinElmer). *Z* stacks were acquired at 0.2 μm intervals and merged images were generated using Volocity software. Deconvolution (Iterative Restoration with 20 iterations) was performed using Volocity software. Images were processed using Adobe Photoshop.

For the detection of UFBs, the cells were treated with siRNA 24 h before a brief cisplatin treatment (1 μM for 1 h), and released into fresh media for 24 h. Cells were then fixed with PTEMF. For the detection of DNA replication in prometaphase, the cells were treated with EdU (10 μM) 30 min before fixation with PTEMF. EdU signals were detected using a Click-iT EdU Alexa Fluor 488 Imaging kit (Life Technologies) according to the manufacturer's protocol.

Flow cytometry. Cells were collected, washed with PBS and fixed in ice-cold 70% ethanol overnight at 4 °C. For DNA content analysis, the cells were washed with PBS and incubated with 50 μL of 100 μg ml^{-1} RNase A (Qiagen) and 300 μL of 50 μg ml^{-1} propidium iodide (Sigma-Aldrich) before FACS analysis. For BrdU staining, cells were treated with 10 μM BrdU for 1 h before being collected. Fixed cells were washed twice in PBS, treated with 2 N HCl for 20 min, and then washed twice in PBS and once in PBS-T (PBS with 0.1% Tween 20 and 0.5% BSA). Cells were then treated with mouse anti-BrdU antibody (Becton Dickinson) for 30 min at room temperature, washed twice and then stained with anti-mouse Alexa Fluor 488 secondary antibody (Thermo Fisher) for 30 min. For the detection of histone H3 pSer10, ethanol-fixed cells were washed twice in PBS and once in PBS-T. The cells were then treated with mouse anti-histone H3 pSer10 antibody (Abcam ab14955) for 30 min at room temperature, washed twice and stained with anti-mouse Alexa

Fluor 488 secondary antibody (Thermo Fisher) for 30 min. For the detection of cyclin B1, cells were fixed with 2% paraformaldehyde in PBS for 10 min followed by cold 70% ethanol overnight. Fixed cells were washed twice in PBS and once in PBS-T. The cells were then treated with mouse anti-cyclin B (Cell Signaling 4135) for 30 min at room temperature, washed twice and stained with anti-mouse Alexa Fluor 488 secondary antibody (Thermo Fisher) for 30 min. Following antibody staining, the cells were washed with PBS and stained with either propidium iodide (for ethanol-fixed cells) or 0.5 μg ml^{-1} DAPI (for paraformaldehyde-fixed cells). Samples were analysed using a FACSCalibur or a LSRFortessa Analyzer (BD Biosciences), and at least 10,000 events were acquired per sample. FACS data were analysed using FlowJo software. Cell doublets and debris were excluded from analysis. Cell cycle population analysis was performed using the Watson pragmatic algorithm with FlowJo software.

Comet assays. Alkaline comet assays were performed using a CometAssay kit from Amsbio (4250-050-K) according to the manufacturer's protocol. Alkaline electrophoresis was performed in a BioRad Mini-Sub Cell GT system (20 volts, 250–300 mA for 30 min), and the comets were stained with SYBR Gold staining solution (Thermo Fisher, 1:10,000 in TE buffer). The percentage of DNA in the tail was measured using ImageJ software with the Comet Assay plugin (https://www.med.unc.edu/microscopy/resources/imagej-plugins-and-macros/comet-assay).

siRNA. The control siRNA (5′-UAAUGUAUUGGAACGCAUA-3′), *BLM* siRNA (5′-CCGAAUCUCAAUGUACAUAGA-3′)[62], *RECQ5* siRNA (5′-CAGGAGGCUGAUAAAGGGUUA-3′)[62], *TREX1* siRNA (5′- CCAAGACCAUCUGCUGUCA-3′)[63], *CTIP* siRNA (5′-GCUAAAACAGGAACGAAUC-3′)[64], *GEN1* siRNA (5′- GUAAAGACCUGCAAUGUUA-3′) were purchased from Eurofins. The *MUS81* siRNA (5′-CAGCCCUGGUGGAUCGAUA-3′ and 5′-CAUUAAGUGUGGGCGUCUA-3′)[29], *SLX1* siRNA (5′-UGGACAGACCUGCUGGAGAUU-3′)[22], *ERCC1* siRNA (SMARTpool ON-TARGET plus L-006311), *MRE11* siRNA (SMARTpool ON-TARGET plus L-009271), *EXO1* siRNA (SMARTpool ON-TARGET plus L-013120), *DNA2* siRNA (SMARTpool ON-TARGET L-026431), *RECQ1* siRNA (SMARTpool ON-TARGET plus L-013597), *RECQ4* siRNA (SMARTpool ON-TARGET plus L-010559), *WRN* siRNA (SMARTpool ON-TARGET plus L-010378), *BRCA2* siRNA (SMARTpool ON-TARGET plus L-003462) and *RAD51* siRNA (SMARTpool ON-TARGET plus L-003530) were purchased from Dharmacon. Cells were seeded one day before siRNA treatment and transfected with 25 nM of siRNA using Lipofectamine RNAiMAX (Life Technologies).

Clonogenic cell survival assay. Cells were first seeded in 6-well plates and transfected with siRNA. After 24 h, cells were either left untreated or treated with the indicated concentrations of cisplatin, aphidicolin or camptothecin for 18 h. Approximately 500 cells were seeded in 6-cm plates and maintained in fresh media for ~10 days to allow colony formation. Colonies were stained for ~5 min with 40 mg ml^{-1} crystal violet solution (Sigma-Aldrich) containing 20% ethanol. Percentage survival was calculated against untreated cells or the control siRNA sample.

Metaphase spreads. To analyse chromosome aberrations, cells were treated with siRNA 24 h before a brief cisplatin treatment (1 μg ml^{-1} for 1 h) and then released into fresh media for 24 or 48 h. Cells were then treated with colcemid (0.2 μg ml^{-1}) for 1 h before being collected, and metaphase chromosomes were prepared as previously described[29]. Segmented chromosomes were scored as those containing two or more indentations per chromosome. For sister chromatid exchange analyses, cells were treated with BrdU (100 μM) for 48 h, and colcemid (0.2 μg ml^{-1}) was added 1 h before collection. The SCE assay was performed as previously described[29].

DNA fibre assays. DNA fibre assays were carried out essentially as previously described[65]. In brief, 293 cells were pulsed with 15 μM CldU (Sigma-Aldrich) for 20 min, washed once with media and labelled with 200 μM IdU (Sigma-Aldrich) for 40 min. Cells were trypsinized, resuspended in PBS and placed on ice. Cells were counted, their concentration adjusted to 500,000 cells per ml, and then mixed 1:5 with unlabelled cells. A total of 3 μL of the cell suspension was placed on top of a glass slide (Superfrost, 90° edges) followed by addition of 9 μL lysis buffer (0.5% SDS, 200 mM Tris-HCl pH 7.4, 50 mM EDTA) and lysed by moving a pipette in a circular motion until the liquid became viscous. The slides were left for 2 min before tilting them at a 10–15° angle to allow the viscous cell lysate to run slowly downwards. The slides were fixed in a methanol:acetic acid solution (3:1) for 15 min at room temperature and air dried before staining. The DNA fibres were denatured by incubating the slides in 2.5 M HCl solution for 60 min. The slides were then washed twice in PBS and blocked in PBS supplemented with 1% BSA for 30 min at room temperature. Slides were stained with rat anti-BrdU (1:1200 dilution; Serotec, BU1/75, OBT0030CX;) and mouse anti-BrdU (1:500 dilution; BD Biosciences, B44) in PBS containing 1% BSA for 2 h, and washed twice in PBS before staining with anti-rat Alexa 594 and anti-mouse Alexa 488 (both 1:500 dilutions; Thermo Fisher) in PBS containing BSA for 1 h. Slides were washed twice in PBS followed by one wash in deionized H_2O and left to air dry in the dark. The slides were mounted with Prolong Gold antifade mountant (Thermo Fisher) and images were acquired on a Zeiss AXIO Imager M2 microscope equipped with a plan-SPOCHROMAT 63×1.4 oil objective (Zeiss) using Volocity software. Images were analysed using ImageJ software.

Statistics and reproducibility. Experiments were not randomized and no blinding was used during data analyses. No statistical methods were used to predetermine sample sizes. Sample sizes were determined based on previous experience to obtain statistical significance and reproducibility. All error bars represent mean ± standard deviation (s.d.) of three independent experiments. Statistical testing was performed using the two-tailed *t*-test. A *P* value of 0.05 was considered as borderline for statistical significance. Each experiment was repeated at least three times, with the exception of the those presented in Supplementary Fig. 2g,h (two experiments performed) and Fig. 4c, Supplementary Figs. 1b,d, 2b–d, 3e,j, 5a,b, and 7b and all western blots (one experiment was performed).

Life Sciences Reporting Summary. Further information on experimental design is available in the Life Sciences Reporting Summary.

Data availability. Statistics source data for Figs. 1–7 and Supplementary Figs. 1–7 are provided in Supplementary Table 1. All data supporting the findings of this study are available from the corresponding author on request.

References

58. Rodriguez-Lopez, A. M., Whitby, M. C., Borer, C. M., Bachler, M. A. & Cox, L. S. Correction of proliferation and drug sensitivity defects in the progeriod Werner's Syndrome by Holliday junction resolution. *Rejuvenation Res.* **10**, 27–40 (2007).
59. Cong, L. et al. Multiplex genome engineering using CRISPR/Cas systems. *Science* **339**, 819–823 (2013).
60. Ran, F. A. et al. Genome engineering using the CRISPR-Cas9 system. *Nat. Protoc.* **8**, 2281–2308 (2013).
61. Essletzbichler, P. et al. Megabase-scale deletion using CRISPR/Cas9 to generate a fully haploid human cell line. *Genome Res.* **24**, 2059–2065 (2014).
62. Paliwal, S., Kanagaraj, R., Sturzenegger, A., Burdova, K. & Janscak, P. Human RECQ5 helicase promotes repair of DNA double-strand breaks by synthesis-dependent strand annealing. *Nucl. Acids Res.* **42**, 2380–2390 (2013).
63. Chowdhury, D. et al. The exonuclease TREX1 is in the SET complex and acts in concert with NM23-H1 to degrade DNA during granzyme A-mediated cell death. *Mol. Cell* **23**, 133–142 (2006).
64. Fugger, K. et al. Human FBH1 helicase contributes to genome maintenance via pro- and anti-recombinase activities. *J. Cell Biol.* **186**, 655–663 (2009).
65. Petermann, E., Orta, M. L., Issaeva, N., Schultz, N. & Helleday, T. Hydroxyurea-stalled replication forks become progressively inactivated and require two different RAD51-mediated pathways for restart and repair. *Mol. Cell* **37**, 492–502 (2010).

nature research

Corresponding author(s): Stephen C. West

☐ Initial submission ☐ Revised version ☒ Final submission

Life Sciences Reporting Summary

Nature Research wishes to improve the reproducibility of the work that we publish. This form is intended for publication with all accepted life science papers and provides structure for consistency and transparency in reporting. Every life science submission will use this form; some list items might not apply to an individual manuscript, but all fields must be completed for clarity.

For further information on the points included in this form, see Reporting Life Sciences Research. For further information on Nature Research policies, including our data availability policy, see Authors & Referees and the Editorial Policy Checklist.

Experimental design

1. Sample size

Describe how sample size was determined.

No statistical methods were used to predetermine sample size. Sample sizes were determined based on previous experience to obtain statistical significance and reproducibility.

2. Data exclusions

Describe any data exclusions.

No data was excluded

3. Replication

Describe whether the experimental findings were reliably reproduced.

All experimental findings were reliably reproduced in multiple independent experiments.

4. Randomization

Describe how samples/organisms/participants were allocated into experimental groups.

No randomization.

5. Blinding

Describe whether the investigators were blinded to group allocation during data collection and/or analysis.

No blinding was applied

Note: all studies involving animals and/or human research participants must disclose whether blinding and randomization were used.

6. Statistical parameters

For all figures and tables that use statistical methods, confirm that the following items are present in relevant figure legends (or in the Methods section if additional space is needed).

n/a	Confirmed	
☐	☒	The exact sample size (*n*) for each experimental group/condition, given as a discrete number and unit of measurement (animals, litters, cultures, etc.)
☐	☒	A description of how samples were collected, noting whether measurements were taken from distinct samples or whether the same sample was measured repeatedly
☐	☒	A statement indicating how many times each experiment was replicated
☐	☒	The statistical test(s) used and whether they are one- or two-sided (note: only common tests should be described solely by name; more complex techniques should be described in the Methods section)
☒	☐	A description of any assumptions or corrections, such as an adjustment for multiple comparisons
☐	☒	The test results (e.g. *P* values) given as exact values whenever possible and with confidence intervals noted
☐	☒	A clear description of statistics including central tendency (e.g. median, mean) and variation (e.g. standard deviation, interquartile range)
☐	☒	Clearly defined error bars

See the web collection on statistics for biologists for further resources and guidance.

Software

Policy information about availability of computer code

7. Software

Describe the software used to analyze the data in this study.	ImageJ 1.50c (with Comet Assay plugin), Microsoft Excel 15.37, GraphPad Prism 7.0b, Adobe Photoshop CS5.1, Volocity 6.3 and FlowJo 10 softwares are used to analyze the data

For manuscripts utilizing custom algorithms or software that are central to the paper but not yet described in the published literature, software must be made available to editors and reviewers upon request. We strongly encourage code deposition in a community repository (e.g. GitHub). *Nature Methods* guidance for providing algorithms and software for publication provides further information on this topic.

Materials and reagents

Policy information about availability of materials

8. Materials availability

Indicate whether there are restrictions on availability of unique materials or if these materials are only available for distribution by a for-profit company.	There is no restriction.

9. Antibodies

Describe the antibodies used and how they were validated for use in the system under study (i.e. assay and species).	rabbit anti-MRE11 (1:1000, Cell signalling 48955), rabbit anti-DNA2 (1:1000, Abcam ab96488), rabbit anti-EXO1 (1:1000, Abcam ab95068), rabbit anti-CTIP (1:1000, Bethyl A300-488A), rabbit anti-RTEL1 (1:1000, Novus NBP2-22360), rabbit anti-RECQ1 (1:1000, Bethyl A300-447A), rabbit anti-RAD51 (1:200, SantaCruz sc-8349), mouse anti-BRCA2 (1:1000, Calbiochem OP95), mouse anti-α-tubulin (1:5000, sigma T9026), mouse anti-FLAG HRP (1:1000, Sigma-Aldrich A8592), mouse anti-MUS81 (1:1000, Santa Cruz sc-47692), rabbit anti-BLM (1:1000, Abcam ab2179), rabbit anti-KAP-1 pSer842 (1:1000, Abcam ab70369), mouse-anti-CHK1 (1:1000, Sigma-Aldrich C9358), rabbit anti-CHK1 pSer317 (1:1000, Cell signalling 2341), mouse anti-histone H2A.X pSer139 (1:1000, Millipore 05-636-1), mouse anti-CHK2 (1:1000, Millipore 05-649), rabbit anti-CHK2 pThr68 (1:1000, Cell signaling 2661), mouse anti-RPA2 (1:1000, Abcam ab2175), rabbit anti-ERCC1 (1:1000, Santa Cruz sc-10785), mouse anti-PICH (1:500, Millipore 04-1540), rabbit anti-GEN1 (1:100, home-made, raised against GEN1 890-908), sheep anti-SLX1 and sheep anti-SLX4 (1:500, gifts from John Rouse), rabbit anti-WRN, rabbit anti-RECQ4 and rabbit anti-RECQ5 (1:500, gifts from Pavel Janscak), rabbit anti-GFP (1:5000, Abcam ab290), mouse anti-cyclin A (1:200, Santa Cruz sc-56299), rabbit anti-MDC1 (1:1000, Abcam ab11169), rabbit anti-FANCD2 (1:1000, Novus NB100-182); human anti-centromere CREST (1:2000, Immunovision HCT-0100), rabbit anti-PICH (1:100, Cell Signaling 8886), rabbit anti-TREX1 (1:1000, Abcam ab185288), rabbit anti-MKLP1 (1:1000, Santa Cruz sc-867), mouse anti-cyclin B (1:100, Cell signalling 4135), mouse anti-histone H3 pSer10 antibody (1:100, Abcam ab14955). Antibodies were validated by western blotting and/or immunofluorescence staining.

10. Eukaryotic cell lines

a. State the source of each eukaryotic cell line used.	293 cell was obtained from Thermo Fisher. RPE1 and U2OS cells were obtained from ATCC. eHAP cell was obtained Horizon Discovery.
b. Describe the method of cell line authentication used.	Cell line authentication was not performed as cells were not listed in the commonly misidentified category.
c. Report whether the cell lines were tested for mycoplasma contamination.	All cell lines were tested negative for mycoplasma.
d. If any of the cell lines used are listed in the database of commonly misidentified cell lines maintained by ICLAC, provide a scientific rationale for their use.	None of the cell lines used in this study are listed in the commonly misidentified category.

Animals and human research participants

Policy information about studies involving animals; when reporting animal research, follow the ARRIVE guidelines

11. Description of research animals

Provide details on animals and/or animal-derived materials used in the study.	No animals were used in this study.

Policy information about studies involving human research participants

12. Description of human research participants

Describe the covariate-relevant population characteristics of the human research participants.	This study did not involve human research participants.

nature research

Corresponding author(s): Stephen C. West

☐ Initial submission ☐ Revised version ☒ Final submission

Flow Cytometry Reporting Summary

Form fields will expand as needed. Please do not leave fields blank.

Data presentation

For all flow cytometry data, confirm that:

☒ 1. The axis labels state the marker and fluorochrome used (e.g. CD4-FITC).

☒ 2. The axis scales are clearly visible. Include numbers along axes only for bottom left plot of group (a 'group' is an analysis of identical markers).

☒ 3. All plots are contour plots with outliers or pseudocolor plots.

☒ 4. A numerical value for number of cells or percentage (with statistics) is provided.

Methodological details

5. Describe the sample preparation.	70% ethanol fixation, followed by propidium iodide/DAPI staining. Detailed description is provided in the Methods section.
6. Identify the instrument used for data collection.	BD FACSCalibur and BD LSRFortessa analyzer
7. Describe the software used to collect and analyze the flow cytometry data.	The data was collected by FACSDiva and analyzed by Flowjo.
8. Describe the abundance of the relevant cell populations within post-sort fractions.	At least 10000 cells were acquired for each sample.
9. Describe the gating strategy used.	FSC/SSC gate was used for gating the population of cells to exclude cell doublets and debris. Asynchronous growing cell population was first run to set up the axis. All test samples were then run in identical condition.

Tick this box to confirm that a figure exemplifying the gating strategy is provided in the Supplementary Information. ☒